D1.1
State of the art and prerequisites report

General information	
Grant agreement number	755500
Start date of the project	01/09/2017
Project duration	48 months
Due date of the deliverable	30/11/2017
Actual submission date	03/10/2018
Lead beneficiary	1 - EDF

Keywords
SOAR

Type	Meaning	
R	Document, report	x
DEM	Demonstrator, pilot, prototype	
DEC	Websites, patent fillings, videos, etc.	
OTHER	Software, technical diagram, etc.	

Dissemination Level		
PU	Public	x
CO	Confidential, only for members of the consortium (including the Commission Services)	

Table of Contents

Table of Figures

Table of Tables

Glossary

Abbreviations/Acronym	Description
CAFE	Cellular Automation Finite Element
DORT	Decomposition of the Time Reversal Operator
FEM	Finite Element Method
FMC	Full Matrix Capture
FOM	Figure-Of-Merit
GBS	Gaussian Beam Superposition
GPSS	Generalized Point Source Superposition
GUI	Graphic User Interface
IAB	Industrial Advisory Board
PWI	Plane Wave Imaging
SEM	Spectral Element Method
SMAW	Shielded Metal Arc Welding
TFM	Total Focusing Method
TRL	Transmission Reception Longitudinal (transducer)
UT	Ultrasonic Testing
WNS	Welding-Numerical Simulation

1 Summary

This report aims to establish the current state of the art in view of complex structured materials and the associated challenges for ultrasonic testing.

After introducing typical metallurgical characteristics of complex microstructures and their effect on the performance of ultrasonic testing, we discuss modelling approaches for the physics involved. This concerns models to predict the material structure of welds, and models to simulate wave propagation and grain scattering in polycrystalline media. Computer modelling tools are identified, which are suited for modification and extension in the course of the project. We distinguish tools based on an effective medium concept requiring low calculation times, which are thus suitable for online application, i.e. during onsite inspections, and tools operating with long calculation times and/or large storage memory requirements, thus to be applied for offline calculations and studies.

The experimental aspects of ultrasonic inspection of complex structured materials are discussed, both in terms of fundamental considerations for the selection of acquisition parameters, and in terms of existing industry standards.

Furthermore, available imaging algorithms and inversion techniques are discussed. The report concludes with a list of open issues and provides a list of available mock-ups in the annex.

2 Introduction

The ADVISE project seeks to advance the ultrasonic inspection of corrosion resistant alloys, in particular austenitic welds and cast austenitic steel, for which conventional ultrasonic techniques suffer from severe performance limitations due to their microstructure, which is responsible for structural noise, attenuation and beam deviation.

Today, the development of an ultrasonic inspection method relies on supposedly representative mock-ups, which are destructively analysed for material characterization. This information is then used to identify the most suitable inspection parameters. The key idea of the ADVISE project is to combine model-predicted information with in-situ characterization techniques to acquire specific information about the structure to be inspected. This information is then used for model-assisted iterative optimisation of customized transducers and associated delay laws, to specify the most appropriate inspection approach, based on the actual material under test. Later, the same information serves in model-assisted diagnostics, to fully exploit the information contained in full matrix capture (FMC) acquisitions.

The project is structured into five technical work packages. This report is a key deliverable of WP1 “Comprehension and modelling”, and compiles information on the current state of the art and the prerequisites for the different tasks at hand. Chapter 3 introduces the metallurgical characteristics of complex structured material, and briefly recalls the associated challenges for ultrasonic testing, which are the raison d’être of the ADVISE project.

Chapter 4 provides a review of the current state of the art of modelling approaches for weld structures, wave propagation, grain scattering theory and wave-defect interaction models. Solidification models for cast austenitic steel have voluntarily been excluded, as they are beyond the scope of the project. The numerical aspects of the modelling approaches presented in Chapter 4 are developed in Chapter 5, which identifies appropriate simulation tools suited for modification and extension for the purposes of the project. It distinguishes tools based on an effective medium concept, requiring low calculation times, which are thus suitable for online application, i.e. during onsite inspections, and tools operating with long calculation times and/or large storage memory requirements, thus to be applied for offline calculations and studies (Task 1.1.3).

Chapter 6 covers experimental considerations when tailoring an inspection to complex structured materials and introduces the existing standards and specifications that govern ultrasonic testing for these materials. Imaging and inversion techniques applied to assess and interpret the acquired ultrasonic data are presented in Chapter 7.

Annex A provides a shortlist of readily available specimens of relevant materials, components and defect types for various industrial targets.

3 Complex microstructures and their significance

3.1 Typical metallurgical characteristics

The morphological properties (orientation, size) and texture of grains of austenitic steel are determined by the solidification process. As the material solidifies, columnar grains are formed which exhibit preferential growth along the gradient of heat loss. Differences in the solidification process for austenitic welds, where expitaxial growth induced by successive weld beads occurs, and cast austenitic steel, where no remelting takes place, lead to different microstructures.

In the case of austenitic welds, there is very considerable spatial variation of the microstructure, including both grain elongation with preferential orientations, and associated with this, spatially defined preferred crystallographic orientations. These details of spatial heterogeneity are at the heart of the complex wave behaviours that will be discussed in relation to weld materials in the following sections. Much work on evaluation of the microstructure of the weld materials and appropriate representations in order to model wave propagation through them have been published, for example [1]–[6]. An important observation arising from this work has been that the formation of the weld creates material such that a cross section through a weld is approximately a plane of material symmetry. This has very conveniently allowed model studies to be conducted in just two dimensions. However, it is also well observed that this is an approximation, and the question remains whether the two-dimensional assumption is a reasonable one. One of the interests of ADVISE is to identify the significance, or not, of including the third dimension in model representations.

On the other hand, in the case of cast austenitic steels, the expectation is for a distribution of grain shapes, sizes and crystallographic texture that is more uniform spatially, with lower tendancy to preferential directions, and the representations for modelling are typically chosen to be homogeneous. Nevertheless, spatial variations do occur, particularly in grain sizes, and these can sometimes be dramatic. The main properties of the microstructure may be identified on an exposed surface using electron back scatter diffraction (EBSD), which derives local crystal orientation from diffraction patterns of electron beam backscattered from a flat and polished sample.

Numerical welding simulation (NWS) using finite elements was primarily developed to determine (undesirable) internal stress and strain due to subsequent heating and cooling in the welding process, but is also able to provide local properties of the resulting microstructure [7].

Once the microstructure is known, it can be used as an input into the analytical models, the numerical wave simulations, or to derive the parameters for scattering models.

A simpler approach on a macro or “morphological” scale is adopted by phenomenological models like MINA, producing orientation of grains and their variation across the weld, correlated with effective material properties.

3.2 Challenges for ultrasonic inspection

The challenges perplexing ultrasonic inspection of welds in austentic steels and austenitic steel or nickel alloy castings originate from their coarse-grained, dendritic (welds) microstructure [8]. Each grain (crystal) is in general anisotropic and the wave velocity is directionally dependent. As long as the grains are randomly oriented and small in comparison with the wavelength of ultrasound, the single crystal anisotropy has no macroscopic effect. In this case, the material exhibits a macroscopic, quasi-

isotropic elastic behaviour. However, as discussed in the preceding section, the two particularly difficult to inspect types of materials used in the nuclear industry, namely austenitic welds and austenitic steel or nickel alloy castings, break the aforementioned conditions.

In weldments of austenitic or nickel-based materials, generally large, elongated grains form, with preferred orientations depending on the cooling conditions following the welding. The formation of such dendritic grains leads to a spatially inhomogeneous, macroscopic anisotropy. On the other hand, grains in castings of interest are often nearly randomly oriented, but the grain size is of the same order of magnitude as the wavelength. These microstructures are responsible for a number of confounding phenomena: attenuation and distortion, backscatter, beam skewing and beam deviation. Without considering them, the inspection could lead to erroneous conclusions and could in extreme cases stimulate a misleading interpretation of ultrasonic indications.

3.2.1 Attenuation and distortion

The term attenuation englobes energy loss due to absorption and scattering. Absorption also takes place in homogeneous media and refers to acoustic energy converted into heat. In homogeneous and isotropic media, attenuation can be described by the attenuation coefficient. In anisotropic media, attenuation is direction dependent, and a complex elastic stiffness tensor is required to characterize attenuation [9]. However, for complex-structured materials attenuation originating from scattering is of primary importance. Scattering takes place at interfaces between materials (grain boundaries) with different acoustic impedance. One consequence is that while passing through subsequent grain boundaries, the energy is diffracted away from the ultrasonic beam. Furthermore, the diffraction depends on the ratio of wavelength to grain size, hence the attenuation changes with frequency. Finally, apart from the loss of amplitude with distance, this frequency-dependent form of attenuation also distorts the signal in the time domain.

3.2.2 Backscatter

Another consequence of scattering at grain boundaries is structural noise, or backscatter. Part of the energy incident upon a grain boundary is reflected and transmitted in directions other than the main ultrasonic beam. Backscatter refers to the scattered ultrasound making its way back to the transducer. Since backscattered ultrasound has taken numerous different paths with different times-of-flight, it manifests itself as background noise throughout the received ultrasound signal, reducing the signal to noise ratio. Backscatter can overlay ultrasonic indications of material defects and potentially screen them off.

3.2.3 Beam skewing

In isotropic media, two wave modes exist, with polarisation (the direction of particle displacement) either parallel (longitudinal waves), or perpendicular (transverse waves) to the direction of propagation of wave energy. Beam skewing, observed in anisotropic materials, refers to a deviation of the polarisation from these ideal directions, and affects the interaction of the sound wave with defects.

3.2.4 Beam deviation

Spatial inhomogeneity of the anisotropic stiffness properties induces a deviation of the beam. For a continuous variation of stiffness properties, deviation can result in a curved beam path, which is particularly evident in welds. If spatial inhomogeneity occurs across regions smaller than the beam

width, beam splitting can also be observed. In all cases, echo localisation becomes impossible without knowledge about the local stiffness properties.

4 Modelling of the physics

Ultrasonic testing (UT) of microstructured media relies on models able to provide insight into the breadth of physical phenomena involved. In this chapter, we discuss fundamental models which attempt to capture mechanisms governing both material structure formation and wave propagation. Whilst such models are often incapable of handling very complex inspection scenarios, they are of key importance to the understanding of the physics. The insights gained from fundamental simulations inform the design of inspection and more elaborate numerical simulations.

Models for wave propagation, scattering and interaction with defects require a-priori knowledge of the material structure. Therefore, both geometrical and phenomenological modelling of weld microstructure is discussed first, followed by the description of the fundamental approaches to understand characteristic features of wave propagation in polycrystalline media and grain scattering. The last section presents a review of wave-defect interaction models applicable to complex welds.

4.1 Models of the material structure

4.1.1 Geometric representations for welds

The first attempts to represent grain orientations in a weld were based on simple geometric observations. The pioneering work was published by Ogilvy [10], who defined grain orientations using analytic functions derived from experimental observations. A few tuning parameters allowed for specifying the rate of change of grain orientations between the chamfer and the centreline. Following similar intuitions, Spies [11] proposed dividing the weld into several transversely isotropic layers, each with a constant material orientation assigned. Other geometrical representations included a simplified model by Langenberg *et al.* [12], who set the grains to be inclinded either at 0 or 45 degrees to the vertical axis, or the approach of Schmitz *et al.* [13] in which analytically defined orientation vectors described the varying grain inclination.

Whilst the models recalled above were found useful for improving prediction of ultrasound propagation through complex welds, they suffered from several shortcomings. Their major weakness was the lack of connection between the physics of welding and the resulting grain orientations.

4.1.2 Phenomenological weld modelling: MINA

A number of efforts have been made to calculate the weld structure from known welding parameters. One successful attempt was the MINA (Modelling anisotropy from Notebook of Arc welding) model [3]. MINA is a phenomenological model, conceived for the specific need of ultrasound wave propagation modelling. It assumes that for this purpose, a description on an intermediate scale between the microscopic scale, where actual grains would be represented, and a macroscopic scale representing passes, is sufficient to accurately simulate the impact of the weld on the ultrasound beam, in terms of deviation, splitting and focusing. Moreover, it is compatible with the information typically available in welding notebooks. The MINA model [3] calculates local grain orientations, based on such parameters as: the chamfer geometry, the number and direction of passes and the electrode diameter for shielded metal arc welding (SMAW). The model accounts for the partial remelting of already solidified passes for each new pass laid throughout the welding process. The obtained two-dimensional mesh of material orientations at a macroscopic scale has been validated by comparison

with macrographs. The two-dimensional approach limits MINA to flat weldings. A more detailed description of this model follows in subsequent paragraphs.

MINA uses a phenomenological approach to determine the stiffness map of the weld. The stiffness map captures local orientations of the grains at a macroscopic scale, but disregards grain partitioning.

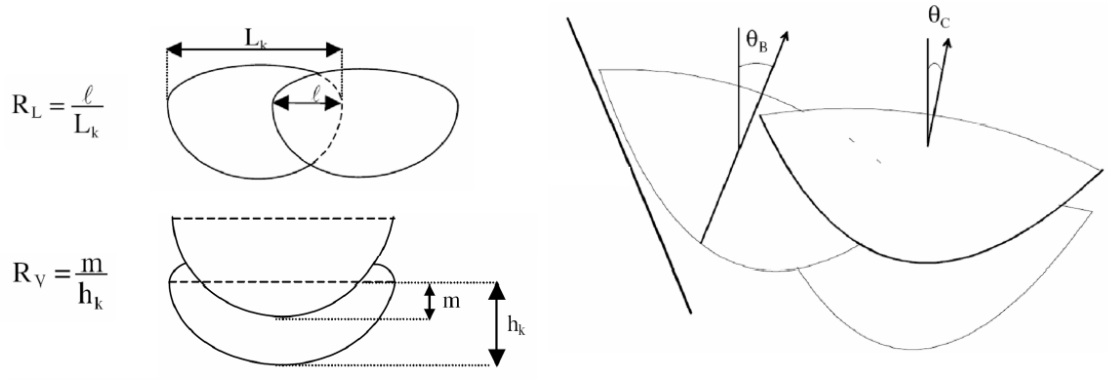

Figure 1: Definition of remelting rates (left) and melt pool geometry (right) in MINA.

MINA modelling starts from the gathering of the information contained in the welding notebook: the order of passes, the electrode diameter and the geometry of the chamfer. A layout of passes can then be constructed. The weld pool geometry is represented by two parabolic curves (Figure 1 right). The thermal gradient – local grain growth direction – is assumed to be perpendicular to the weld bead boundary. The two angles Θ_B and Θ_C allow to take the inclination angle of the electrode into account and denote the inclination of the temperature gradient for passes leaning on a previous pass or the weld geometry. The ThetaC parameter governs the inclination of a pass located at the center of the welding, which means a pass which does not touch the weld chamfer. This parameter has been shown to be highly sensitive to the welding position and can be determined for typical welding positions after metallographic examination. Successive pass heights are assumed proportional to the electrode diameters.

The partial remelting of the previous pass by a newly deposited pass is simply described in terms of lateral and vertical remelting rates R_L and R_V, as indicated in Figure 1 left, which can be obtained by analysis of macrographs of a number of welds.

The grain growth in austenitic welds mainly proceeds from the conjunction of two physical phenomena: the selective growth and the epitaxial growth. On the one hand, thanks to epitaxial growth, a crystallite growing in a new pass assumes the crystallographic orientation of the underlying grain. The phenomenon occurs when the heating conditions do not produce recrystallization in the previous pass. On the other hand, the selective growth phenomenon tends to select the grains which exhibit a <100> crystallographic direction aligned with the local thermal gradient in the welding bead. Finally, the MINA model tries to reproduce the temperature gradient by reproducing the shape of the welding bead in any pass (neglecting the Marangoni effect).

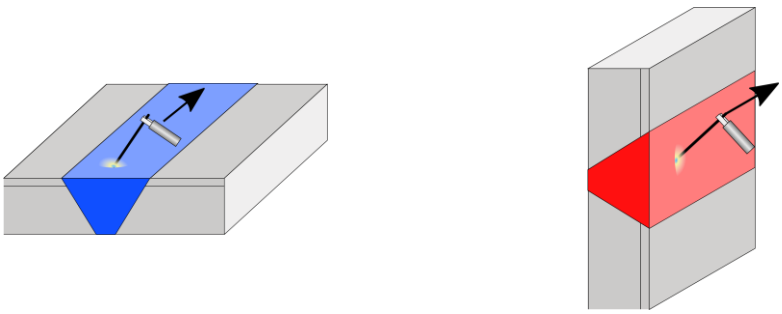

Figure 2: Flat welding position (left) and horizontal vertical welding position (right).

In terms of geometry, MINA can manage different 2D weld shapes: simple V, K or X-shaped. In the case of a X or K-shape weld with reverse welding, two V welds are modelled separately and concatenated. This 2D approach assumes that the plane section across the weld is a plane of material symmetry.

The model has been validated experimentally for multipass welds with shielded electrodes and up to 60 passes, showing an average accuracy of 10 to 15 degrees for the grain orientation – after macrographs. The MINA model has also shown very good results in predicting the differences of stiffness maps of two identical welds, one welded in flat position, the other one welded in horizontal welding position (see Figure 2).

MINA has proved to be a very versatile tool applicable to a variety of contexts. For weld characterisation it may be used to produce an educated first guess on the structure of a weld, which can then be successively refined using in-situ measurements.

For further use in Finite Element codes for ultrasound propagation simulation (e.g. ATHENA, Pogo), the initial stiffness mesh of MINA, which is typically discretized to a cell size of 0.25 mm, is coarsened in a larger square grid, the typical size of which varies from 5 mm to 0.5 mm, depending on the frequency of the inspection. Table 1 summarises the MINA input parameters.

Table 1: Basic characteristics of the MINA model

Parameter	MINA model	Solidification model
Number of passes	x	x
Order of passes	x	x
Electrode diameter	For each pass	x
Pass thickness	-[1]	-
Welding speed	-	x
Weld joint shape	V,K[2],X[2]	x
Energy	-	x
Remelting rate	Lateral, vertical	-
Electrode inclination[3]	x	x
Epitaxial and selective growth	X[4]	-
Welding type	SMAW	GTAW, SMAW, SAW
Pre-heating and interpass temperature	-	x
Temperature dependent material properties, 20°C to melting-point	-	x [5]

1) Derived from electrode diameter
2) Obtained by stacking two v-shape welds
3) enables to define the welding position from flat to horizontal vertical.
4) Described in terms of the number of iterations of a macroscopic model
5) Young's modules, Poisson's ratio, Flow cuves, thermal expansion and conductivity, specific heat capacity, electrical resistance in case of spot welds, phase transformation kinetics

4.1.3 Cast components – microstructure synthesis

Grains in cast components are typically randomly oriented and no strong preferential alignments are observed. The microstructure is governed by a number of parameters such as grain size, its distribution, sphericity, etc. For the purpose of scattering and attenuation calculations, a two-point correlation function is particularly useful. Two-point correlation function describes the likelihood that two randomly selected points separated by a chosen distance belong to the same grain. This description is widely used in analytical and semi-analytical modelling of the scattering phenomena, e.g. in [14].

For numerical modelling, a more explicit modelling approach was necessary. Over the past few decades, Voronoi tessellations have been used to generate microstructures similar to those occurring in nature and are now widely accepted by the community [15]. A number of established software packages and workflows exist to synthesise microstructure based on their specified morphological parameters, such as grain size distributions or sphericities, to name just a few [16], [17]. Synthesised microstructures can be meshed and used in finite element packages to simulate ultrasound propagation. For this particular application, a number of additional factors must be considered when choosing element shape, size and other solver parameters [18].

4.2 Models of wave propagation in polycrystalline media

A complexity of phenomena involved in ultrasound propagation through a polycrystalline medium remains a longstanding modelling challenge. Two, coexistent and often merging approaches have been adopted by scientists and engineers. One attempts to account for these effects in ultrasonic simulation codes and imaging methods, the other focuses on studying the fundamental phenomena themselves.

First approaches belonging to the former group have been presented in Refs. [19]–[21]. Furthermore, ultrasonic scattering and (viscoelastic) damping in strongly attenuating media, such as cast materials and fiber-reinforced composites, have been considered using phenomenological descriptions in simulation techniques and in imaging algorithms [22], [23].

Going beyond such phenomenological models requires proper consideration of microstructural properties such as e.g. grain size distributions, which leads naturally to the second group - fundamental modelling. Despite the fact that the fundamental approaches rely on a number of approximations regarding multiple scattering, randomness of the medium, etc., the understanding of the elastodynamic behaviour of such media advanced considerably over the last few decades. Ultrasound propagation and, most importantly, scattering models at a crystal level are briefly summarized below.

4.2.1 Wave velocity and beam deviation

Wave propagation in a single, generally anisotropic, crystal is governed by the famous Christoffel's equation which was formulated as early as in 1877 [24]. It can be solved as an eigenvalue problem of a set of three homogeneous linear equations, where eigenvalues are the velocities of the possible

waves, and associated eigenvectors correspond to the polarisations. Christoffel also introduced the notion of the slowness surface as an illustration of the direction dependency of wave velocity, from which a graphical method for the determination of reflection and refraction of plane waves at interfaces between two media can be derived. Today the Christoffel equation is a staple in textbooks on ultrasound in anisotropic media.

The problem of beam deviation is particularly relevant for welds, where the preferred grain orientations lead to an anisotropic, spatially inhomogeneous structure. How the ultrasonic ray deviates while propagating through subsequent grains can be modelled through subsequent applications of a scattering model, such as the one presented by Rokhlin and Adler [25]. This is a basis for a number of ray tracing models [10], [26], [27] (other ray tracing approaches are discussed in Section 5.2.1).

4.2.2 Scattering: attenuation and structural noise

Based on the number of publications over the past few decades and the urging enquiries from practitioners, one can judge that good understanding of scattering is the key to bring ultrasonic inspections of complex structures to the next level. The early approaches to study scattering were reviewed in the 1960s by Papadakis [28]. A very important model, the so-called “unified theory”, capturing the three scattering regimes: the Rayleigh, stochastic and geometric was presented by Stanke & Kino [14] in the 1980s. At about the same time, Hirsekorn addressed this problem too. Her analytical considerations have dealt with calculations in view of frequency dependence of phase and group velocities as well as the inclusion of grain orientation distributions (texture) for the specific case of grain shape isotropy assuming an average grain size [29]–[32]. A few years later, Weaver arrived at an analogous dispersion equation to Stanke & Kino’s, but expressed in the spatial frequency domain [33]. More recently, an ultrasonic inspection technique for cast components made of non-ferrous materials has been elaborated, where the detectability of pores depending on the size and porosity percentage is calculated [34], [35].

In another recent approach, Dobrovolskij *et al*. [36] combined a model of randomly distributed spherical scatterers with the Generalized Point Source Superposition (GPSS) simulations to predict scattering coefficients for microscopically inhomogeneous materials.

Ultrasound scattering for a variety of configurations was also extensively studied by Rokhlin and his research group. Among others, they derived backscattering and attenuation coefficients for polycrystals with uniaxial crystallographic texture and elongated cubic crystallites described by a modified Gaussian orientation distribution and presented a far-field approximation [37]–[39]. They also pointed out that second order multiple scattering must be taken into account when deducing dispersive ultrasonic velocity and attenuation coefficients for materials with no equiaxed grains with arbitrary elastic symmetry. The evidence of multiple scattering effects was also stressed by Thompson *et al.* [40] in their theoretical overview of elastic wave propagation in polycrystals which also includes new experiments supporting this fact.

The advance in numerical modelling over the past decades, largely related to the technological advance, created an opportunity to support fundamental modelling of scattering, given how difficult it is to obtain reliable experimental data. Since the exact description of the randomness of the medium is seldom known and measuring coherent waves in scattering media remains a challenge, finite element simulations can act as virtual, fully controllable experiments. Recently, both the unified theory [14] and another second order model were successfully validated using numerical models [41], [42].

The grain scattering models discussed above typically consider the interaction between plane waves and the microstructure. In order to compute structural noise, their outputs need to be associated with models of the ultrasonic fields in NDE experiments. Several approaches to the computation of structural noise have been proposed in the literature. Two types of computations can be distinguished.

The first type produces examples of structural noise. Empirical approaches have been developed by Gustafsson and Stepinski [43] and by Chatillon *et al.* [44]: they do not rely on a grain scattering model and their parameters have to be set empirically to fit the desired noise. Yalda *et al.* [45] proposed a more complete but cost-intensive approach where they model the material as a collection of single crystals and explicitly compute their echoes. Dorval *et al.* [46] proposed a faster approach where the number of scatterers is smaller than the number of crystals and their amplitude is adjusted, in order to aim for the Figure-of-Merit (FOM) of the polycrystal.

The second type of computation produces statistical indicators of noise instead of examples of it. Thompson *et al.* [47] discussed the relevant statistics and gave expressions in the single scattering approximation, based on a measure called the Figure of Merit (FOM). Turner and co-workers [48], [49] also computed statistical properties of the noise in the single scattering approximation, but then extended their formalism to account for higher orders of scattering and also to predict time domain signals for realistic testing configurations. The modelling of multiply scattered ultrasonic noise remains a complicated problem, where no reliable methods are established, except for numerical finite element simulation.

4.3 Models of the wave-defect interaction

To evaluate the performance of UT inspection techniques, the simulation also requires the modelling of waves scattered by defects. Flaw measurement system models have been developed to predict the results of the ultrasonic inspection in a range of applications [50]–[52]. The research in flaw scattering focused mainly on semi-analytic (SA) approximations that lead to a shorter computation time and are currently the most popular technique for intensive UT simulations. The different SA scattering models can be classified according to the scatterer geometry: crack-like flaws (consisting of flat facets), cavities and solid inclusions.

Two classical SA scattering models are used in the literature to simulate wave interaction with cracks: the Kirchhoff approximation (KA) [53] and the Geometrical Theory of Diffraction (GTD) [54]. They are based on different approximations and have complementary regions of validity. KA is used to deal with reflections from planar-like cracks as well as volumetric voids, such as spherical or hemispherical holes and Side Drilled Holes (SDH) [55]. KA is particularly suitable for simulating direct reflection from flaws as well as corner effects [51], [53] and can also deal with anisotropy [56] and impedance (non-rigid) interfaces [57]. GTD is suitable for simulating scattering by crack edges, away from specular angles and forward paths. Unlike GTD, KA does not model edge diffraction correctly and unlike KA, GTD is not suitable for describing specular reflections. Moreover, the GTD coefficients diverge near incident and reflection shadow boundaries.

Chapman [53] has presented the first complete system model, which could use either KA or GTD to simulate the ultrasonic response of a planar crack in an isotropic material but it had been limited to 2D configurations, in which the crack is perpendicular to the incident plane. KA models have been then extended to 3D [51], [55]. Several GTD-based system models [58], [59] have also been developed for 2D configurations, particularly time of flight diffraction (TOFD), in which cracks are detected using their

edge diffracted echoes. The GTD-based system model [60] then deals with 3D CAD-defects and 3D inspection configurations.

Choosing between models based on KA or GTD requires expertise. Therefore, the research steered towards the development of uniform generic models dealing with both specular reflection and diffraction [61] (in contrast to Kirchhoff and GTD): Physical Theory of Diffraction (PTD), Uniform Theory of Diffraction (UTD) and Uniform Asymptotic Theory (UAT). These models were compared with each other numerically for both rigid [62] and elastic scatterers [63]. Adapted to elastodynamics, a PTD-based system model [61], [64] is henceforth proposed for simulating the ultrasonic response of crack-like defects. The newly developed "elastodynamic" UTD [65] which uses ray tracing, is a particularly practical method and is much faster than UAT or PTD (for very large scatterers).

Concerning cavities, the developed 3D Kirchhoff model simulates these defects but does not take into account the creeping waves propagating along their surface. For that purpose, an exact analytical model (SOV/Separation of Variables) has been implemented and validated [51], [55].

Solid inclusions can be simulated by two kinds of scattering models: the first kind is again the so-called SOV methods using a closed-form solution only for spherical inclusions [66]–[68] and the other, valid for relatively varied geometries, gathers methods based on the Born approximation. The Born approximation is a low frequency and weak scattering approximation. However, in practice , it may be applicable under a wider set of conditions (higher frequency or higher contrasts of density and elastic constants between the host and inclusion materials) using some improvements: doubly distorted Born [66] or modified Born model.

5 Numerical simulation

The simulation of ultrasonic non-destructive testing, in particular weld inspection of nuclear power plant components, represents an important aspect for test planning and improving the detection capabilities of existing, as well as of newly developed, inspection techniques. With the help of simulations, it is possible to determine and optimize important testing parameters such as wave mode, frequency, transducer type and inclination angle before the actual measurement is performed.

For the calculation of A-, B- and C-scans several simulation techniques have been used so far, e.g. ray tracing, point source superposition, Gaussian beam superposition ('multiple Gaussians'), the CIVA-pencil method and EFIT (Elastodynamic Finite Integration Technique). However, all these codes do not take the scattering by the polycrystalline microstructure into account explicitly. Engineering practice clearly shows that for strongly scattering media, like the austenitic base material and the weld area, this interaction needs to be considered.

While the fundamental models described in Chapter 4 address these phenomena separately, they cannot provide a complete simulation of a complex inspection scenario. One of the important aspects of this project is to close this gap in current simulation methodology. The goals are

1. to calculate the relevant scattering coefficients analytically in order to determine the smallest detectable size of circular disc defects in different microstructures;
2. to expand the semi-analytical and numerical simulation techniques in such a way so that not only defect echoes and backwall echoes, but also time-domain grain scattering in A-Scans can be incorporated;
3. to support and validate theory and simulation by appropriate experiments.

In consequence, a better flaw detection sensitivity and an improved interpretation of echo indications is expected.

Gaining a better knowledge of weld properties used in UT inspection modelling, relies critically on the simulation of the welding process itself. During the past years, the development in welding-numerical simulation (WNS), including virtual microstructures has largely evolved. As a first part, an overview of the different approaches to obtain microstructure properties is presented. Following from that, modelling tools dedicated to ultrasonic wave propagation are discussed by considering both microscale and macroscale descriptions of welds.

5.1 Welding formation simulations

Phenomenological models, such as MINA, are extremely useful in practice and simple to use, but at the same time bound by several limitations. For instance, MINA is valid only for metal arc shield welding and assumes that all modelled effects are invariant in the weld direction. Most importantly, however, grain size and its distribution are not predicted. One possible way to address these issues are true solidification models, working on a microscopic scale below the size of a dendrite.

Several approaches have been proposed in the literature to model weld microstructures considering specific simplifying hypotheses regarding grains geometry or orientation [7], [69]–[77]. One method is based on molecular dynamics theory. Molecular dynamics simulations give information at the atomic scale. This includes a comprehensive tracking of all atomic positions and velocities from which detailed defect structures and system thermodynamics can be calculated. This approach has been successfully

used to determine diffusivities that can be incorporated into meso-scale simulation techniques, such as kinetic Monte Carlo. The finite element method is useful for solving problems in solid mechanics, heat transport, and other fields. However, finite element simulation is primarily a continuum technique and is not well-posed, by itself, to simulate the microstructural mass transfer and evolution inherent in the welding process. Therefore, a method situated between the scope of molecular dynamics and finite element methods is required. It is for this reason that the Kinetic Monte Carlo Approach is an ideally suited simulation technique for modelling grain growth under welding [78]–[82].

Another approach is Cellular Automation to simulate the molecular dynamics, the Cellular Automation – Finite Element (CAFE) model gives the opportunity to develop relevant microstructures considering complex phenomena at micro-scale such as individual nucleation processes, growth kinetics and grains interaction [83]–[85].

The finite element method (FEM) lies at the other extreme and is invaluable for solving problems in solid mechanics, heat transport, and other fields, but its inherently continuum nature makes it ill-suited in situations where atomic or microstructural details are important. It is difficult to model the welding by the finite element method. Due to the intense concentration of heat in the heat source of welding, the regions near the weld line undergo many boundary conditions such as clamping force, heat transfer, heat source etc., so predicting three-dimensional weld deformation is a major topic for welding a variety of engineering alloys. The most important problem is the modelling of the solidification. The solidification of alloys typically occurs via dendritic growth in an undercooled melt because very high thermal gradients and high temperatures are reached within the weld pool [86], [87].

The modelling of the welding process is essential to understanding the weld pool formation. As the heat source interacts with the material, the welding process results in three distinct regions in the weldment. These are: the fusion zone, also known as the weld metal, the heat affected zone, and the unaffected base metal. The fusion zone is created by heating above the melting point during welding process. The weld microstructure development in the fusion zone is more complicated because of physical processes that occur due to the interaction of the heat source with the metal during welding, including re-melting, heat and fluid flow, vaporization, dissolution of gasses, solidification, subsequent solid-state transformation, stresses, and distortion. These processes and their interactions profoundly affect weld pool solidification and microstructure. During the solidification process, the austenitic phase forms long columnar grains which grow along the directions of maximum heat loss during cooling [87]. Figures 3 and 4 illustrate the approach.

The extensive columnar grain structure in some austenitic welds differs greatly from that in ferritic welds. Generally, during the process of welding, beads are produced, in which grains grow along the maximum thermal gradient when cooling. This approach is suitable for the determination of a realistic grain orientation [86], but does not include information about grain size. In order to capture the correct grain orientation evolution a number of temperature dependent material properties are required. For pragmatic, sufficiently efficient and not time-consuming determination of grain size, further investigation is needed to reduce the needs for detailed molecular dynamics simulations.

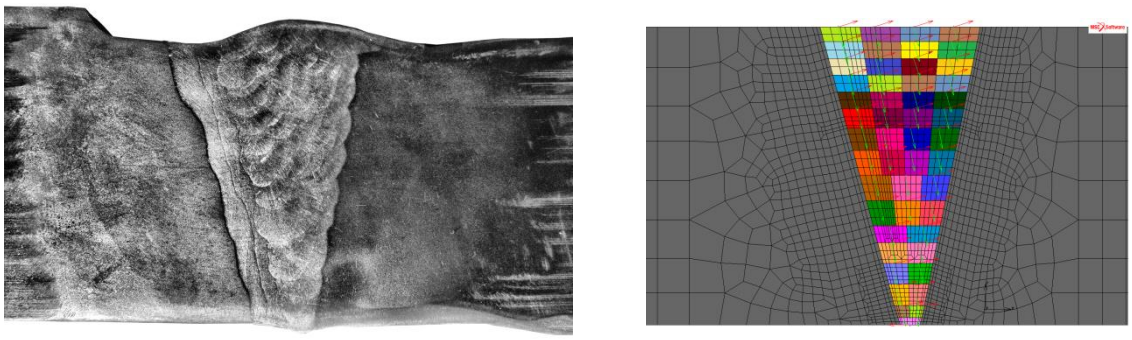

(a) (b)

Figure 3: Illustrative numerical simulation set-up for a dissimilar weld in a steam generator: (a) Investigated specimen; (b) FE mesh of welding simulation [86]

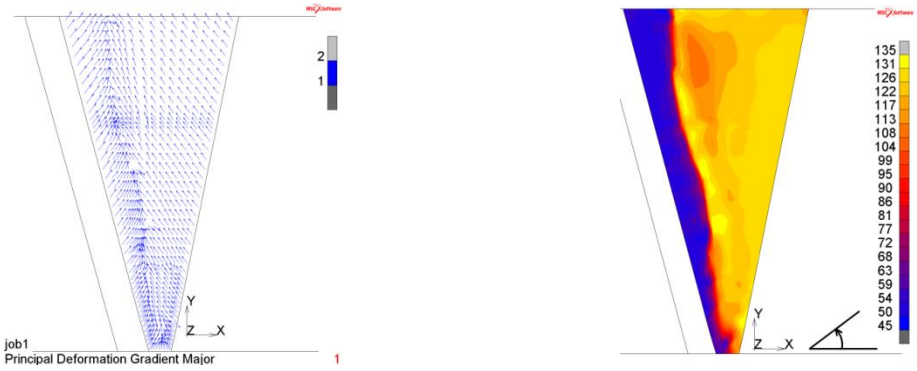

(a) (b)

Figure 4: Results of the illustrative numerical simulation of a dissimilar weld: (a) Modelled orientations as vectors; (b) Contour plots of modelled orientation (45-135°) [86]

5.2 Wave propagation simulations

5.2.1 Semi-analytical methods for online use

Analytical methods apply closed-form solutions to the modelling of propagation and scattering of elastic waves, and as such are limited to a number of canonical problems for which such closed-form solutions exist. Semi-analytical techniques try to overcome these limitations by decomposing the actual problem into elementary solutions, integrated over a problem boundary. These methods overcome two drawbacks of purely numerical tools, i.e. the discretization of the problem domain (which can be prohibitive for 3D problems) and the associated computation time.

An analytical solution for the transient radiation of a planar circular transducer (“piston” transducer) was first presented by Stepanishen [88], [89]. The approach, which is based on the Green’s function development in the time domain, uses a transformation of coordinates to obtain analytical solutions for three different regions for the evaluation of the resultant surface integral. Stephanishen expressed the impulse response as a time-dependent velocity potential for a spatial point in the observation domain. The resulting integral equation is valid for arbitrary transducer shapes and can be solved analytically for the special case of a piston transducer. A convolution of the resulting impulse response function with the excitation signal yields the acoustic pressure in the time domain for a given observation point. Stephanishen’s approach supposes uniform excitation of the transducer surface

(thus called piston mode). For non-uniform excitation and/or arbitrary transducer shapes, the surface integral must be solved numerically.

For the case of orthotropic materials with arbitrary spatial orientation of the symmetry axes, three-dimensional elastic wavefield calculation has been addressed in [90]. Based on a mathematical formulation involving Green's dyadic displacement tensor function, appropriate evaluation resulted in a representation of the displacement vector of transducer wavefields in anisotropic media which is convenient for effective numerical computation. With respect to bulk wave propagation, the numerical evaluation of Green's dyadic function is circumvented by applying a reciprocity-based approach, which is valid in the (point source) far-field. The presented formulation involves characteristic quantities obtained from plane wave theory and appears as a point source superposition representation including the respective point source directivities. Thus, it is in the same form as a corresponding formulation for scattered elastic wavefields [50]. This Generalized Point Source Superposition technique can be applied to cladded components [91] as well and allows to consider isotropic, transversely isotropic and orthotropic elastic material properties including attenuation [92]. The calculations can be performed for single as well as multiple element transducer geometries relevant for the various ultrasonic inspection techniques [93].

To perform wave field calculation for inhomogeneous, anisotropic materials such as austenitic and dissimilar welds, the Gaussian Beam Superposition technique has been elaborated [11], which can be applied to planar and focused transducers with circular or rectangular apertures [94], [95].

At the time when the first geometrical models for weld structure were created, ray tracing appeared as a promising tool for supporting ultrasonic inspection of complex welds. Probably the most known ray tracing model presented in [10] revealed well deviated beam patterns, allowing for pulse-echo rays and reflections from defects to be identified. Following from these achievements, another ray tracing model, based on the Fermat principle, was developed at Imperial College London [96]. In that model, according to a chosen time step, the propagating ray is incident upon subsequent fictitious boundaries defined as lines connecting areas with the same grain orientations. The ray is refracted at each interface according to the model by Rokhlin et al. [25]. Different grain orientation descriptions - geometrical or MINA [97] – can be used, offering visual insights into ultrasonic beam paths and areas inaccessible for inspection. Applications of this model to improved reflector sizing and location in inhomogeneous welds were demonstrated in [98].

Ray tracing applied to complex welds belongs to a much more general class of fundamental algorithmic problems related to shortest-path finding. Two generic, efficient path finding algorithms, known as the Dijkstra and A* methods were recently used for modelling ultrasound in welds at the University of Bristol [99], [100]. They were shown to deliver fast results with a relatively small effect on accuracy, and their formulation is particularly helpful for supporting array imaging scenarios.

The simulation tools for UT wave propagation implemented in the CIVA integration platform are mainly based on the Dynamic Ray Tracing (DRT) formalism developed by geophysicists [101], [102]. This approach is well-suited to deal with various complex-shaped broadband transducers and phased arrays, commonly used in UT inspections. However, the pencil method implemented in CIVA was initially limited to isotropic and anisotropic homogeneous domains [103], [104]. To adapt this ray model to complex weld inspection scenarios, it has been extended to account for a smoothed inhomogeneous anisotropic material [105]. Due to property variations, ray paths are then no longer straight but curved as shown in Figure 5.

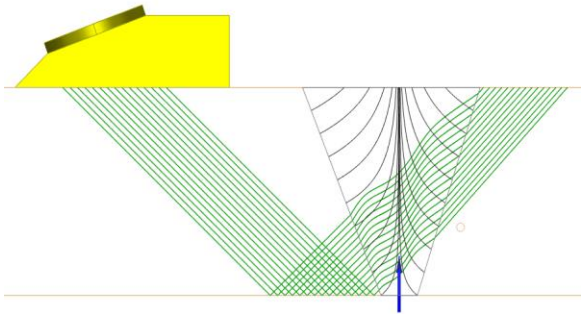

Figure 5: Curved ray paths computed in a V-shaped weld defined by the closed-form expression proposed by Ogilvy [10]

The material attenuation on ultrasonic waves in CIVA can be defined in two ways: the modal description and the "global" description (see Figure 6):

- The modal description allows for defining the attenuation properties according to the wave mode independently. Practically, it is a set of variables depending on the wave propagation direction with respect to a chosen axis (in our case the grain orientation).
- In the global description, the attenuation is represented by the imaginary part of the stiffness tensor enabling the attenuation factor depending on wavefront direction and wave mode to be obtained. The approach used to apply this formalism with ray tracing techniques is explained in detail in [106].

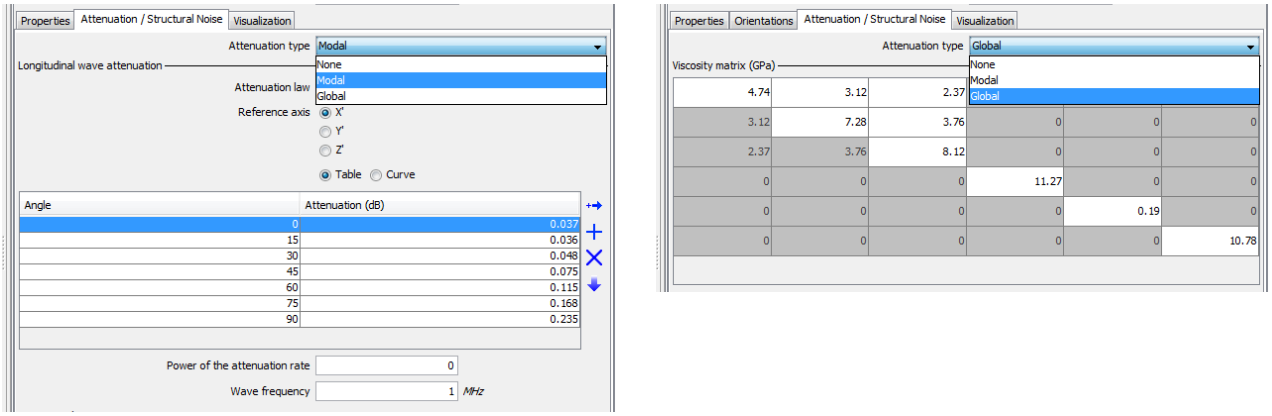

Figure 6: CIVA GUI panels to define attenuation types

5.2.2 Finite element models for offline use and other numerical approaches

Purely numerical tools for elastodynamic wave propagation problems operate directly on the fundamental equations of motion, and appeared first for seismic [107] and non-destructive testing applications [108], [109] in the 1980s, as a complement to analytical methods limited to canonical problems.

For strongly heterogeneous media, which are the focus of the ADVISE project, low order finite elements and a structured (regular) mesh have a number of advantages:

- the regular mesh allows for a constant time step and an explicit time scheme, and a straightforward stability condition;
- a structured mesh with first order elements allows for mass condensation, generating a block-diagonal matrix which is easy to solve for given boundary conditions.

On the other hand, a structured mesh does not lend itself to the representation of complex geometries, which concerns both the component geometry as well as cracks within the component.

The most important numerical tools used for ultrasonic numerical simulation in complex media are reviewed in this section. It is worthwhile to note that these tools are starting to be used for realistic simulations with representation of the material at grain scale, which shows their promising potential to simulate all aspects of the propagation behaviours in detail, both for welds and cast materials.

5.2.2.1 ATHENA

In the finite element code ATHENA, EDF has chosen to combine a first order regular mesh scheme with the fictitious domain method [110]–[112]. In this approach, the regular mesh is used to describe the geometry of the part to be inspected, including the heterogeneous material structure. The fictitious domain method enables to impose a displacement discontinuity along an arbitrary geometry superimposed on the regular, and is used to describe crack-like defects, which otherwise would have to be described within the confines of the regular mesh. This method has proven to extend the use of a 2D code significantly, as it enables the description of thin cracks with branches such as stress-corrosion cracks (SCC), but lacks robustness in its 3D version.

In principle, numerical methods require a discretisation of the entire problem domain. In order to reduce the size of the problem, absorbing boundary conditions are usually provided. While early implementations [113] suffered from reflections produced at large incidence angles, the introduction of perfectly matched layers [114] in the 1990s, first for electromagnetic finite element models and later adapted for elastodynamic problems, reduced the issue [115] except for certain propagation directions in anisotropic materials, and for grazing incidence angles.

In standard finite element methods employing a regular grid, defects must be represented in an approximate way within the limits imposed by the resolution of the regular mesh. One way to overcome these limitations, which affect both the shape and the thickness of possible defects, has been proposed in the form of the domain embedding method, sometimes referred to as the fictitious domain method, and implemented in ATHENA for the problem of scattering by perfect reflectors of an arbitrary shape [111]. This approach consists in extending the solution inside the object artificially, to coincide with the simple rectangular domain corresponding to a cell of the regular mesh, accounting for the boundary condition through the introduction of a new auxiliary unknown defined only at the scatterer's boundary. It should be noted that the fictitious domain method may introduce spurious propagating modes due to the enrichment of the approximation space, suppression of which requires artificial absorption to be incorporated. More recent finite element implementations seem to be in favour of a mesh refinement or unstructured grids instead of the fictitious domain method.

5.2.2.2 Pogo

The finite element package Pogo [116] was developed at ICL with the specific focus of doing fast, large time domain simulations of elastic wave propagation. The key to achieving this is the use of Graphics Processor Units (GPU) to perform highly parallel computations with optimised use of memory. It uses the so-called explicit central difference finite difference scheme for the time marching, with diagonal mass representation of the masses of the elements. This combination allows for the computation at each node at each time step to be dependent only on its immediate neighbours, without any matrix inversions, which is perfect for the hugely parallel calculations for which the GPU architecture is well tuned. The capacity for the spatial model is then governed by the total memory of the GPU facility, while the time stepping speed is typically two orders of magnitude faster than is achieved on conventional CPU facilities. Pogo utilises either regular structured, or free, unstructured meshes, in 2D or 3D. The structured meshes allow for the largest models, reaching 1 billion degrees of freedom in 3D

and 3.2 billion in 2D. The unstructured meshes are not able to achieve this size of model, but on the other hand they can capture the full shape of any defect or component geometry. Absorbing boundaries in Pogo are formulated based on the stiffness reduction method [117] which is a further development of popular absorbing layers with gradually increasing damping.

Pogo models have been used to simulate grain scattering attenuation and wave speed dispersion in polycrystals, in both 2D and 3D. Studies comparing free and structured meshes for these simulations have shown that either approach works effectively [18], after which most of the subsequent work has used structured uniform meshes for their ease of deployment. Validations have been performed by comparison with well-respected analytical models in the literature [41]. Pogo has also been used to assess the implications of a 2D assumption in comparison with the full 3D [118].

5.2.2.3 SEM for elastic waves

The Spectral Element Method (SEM) is a specific high-order method using mass-lumped finite elements where the mass matrix is diagonal by construction. The SEM has been initially used in computational fluid dynamics [119]. Its extension in elastodynamics was proposed for 1D and 2D problems [120]–[122] and extended in 3D initially for seismic wave application [123]. A complete study on both accuracy and stability for more general wave propagation schemes is done by Cohen [124]. It has been proved that this technique requires less degrees of freedom for the same accuracy than conventional FEM [125].

Since 2010, CEA develops a high order spectral FE-code dedicated to UT inspection modelling [126]. The approach used to define a UT scene is based on an arrangement of geometrical structures, called macro-elements (ME), using a domain decomposition technique [127]. Each ME is defined as a potentially nonlinear deformation of a reference cube bearing a predefined hexahedral mesh. Then, the complete scene is built as a set of MEs communicating with each other using the mortar element method [127]. The distinctive feature of this approach lies in an optimal data architecture taking into account the specific domain decomposition [128]. Typically, the so-called stiffness matrix is never to be assembled, but is only represented as a set of local – i.e. per mesh element – matrices and the manipulation of these local matrices are performed in parallel, thus dramatically decreasing CPU time and memory loads allowing 3D computation on standard workstation.

However, the use of high-order finite elements requires a certain spatial regularity of the material properties. This approach is thus only appropriated for a description at the macro scale where variations of the equivalent material properties are of the order of a few fractions of a wavelength.

6 Experimental ultrasonic testing

The ultrasonic inspection of cast or welded austenitic components is a long-standing issue and is known to be difficult or, in some cases, even impossible. This chapter starts with a discussion of the different transducer technologies and configurations as well as acquisition techniques, from which the practioner can choose for the inspection problem at hand. As with any inspection technique, the choice is often a compromise between competing characteristics, including economical aspects in terms of complexity. We also present the existing standards and specifications that govern ultrasonic testing of complex structured materials.

6.1 Transduction

6.1.1 Piezoelectric transducers

Piezoelectric transducers, often referred to as PZT (for lead zirconate titanate) transducers, rely on the piezoelectric effect for transmission and reception. In these materials, application of an electric field generates a deformation of the material, which is used in transducers to produce a (in general) pressure wave. The opposite phenomenon is used in reception: deformation of a piezoelectric material results in the generation of an electric charge. Strictly speaking, transmission exploits the inverse piezoelectric effect.

Piezoelectric transducers require to be in contact with the part in order to transmit ultrasound, either directly (contact transducers) or through a coupling medium (generally water). Shear waves are in general not excited directly, but through mode conversion of incident longitudinal waves. This limits piezoelectric transducers to the generation of shear waves with vertical polarisation (SV).

The excitation of a piezoelectric disk would produce both forward and backward energy radiation. For practical purposes, a transducer therefore contains a damping material behind the piezoelectric element, which also strongly reduces reverberations of the pulse.

In ferritic materials the preferred wave mode for the inspection of welds is the shear wave with beam angles in the range of 40° to 60°, since they do not suffer from energy loss by mode conversion upon reflection at the half skip distance, as opposed to longitudinal waves. Furthermore, longitudinal (L) waves produced by an angle beam transducer with an incidence angle below the first critical angle also produce an additional shear wave beam by refractive mode conversion, which complicates interpretation of signals.

In austenitic materials, however, this obvious advantage is counterbalanced by the fact that shear vertical waves, as produced by an angle beam transducer, are considerably more affected by the weld structure in terms of beam skewing and scattering than longitudinal waves.

6.1.2 EMAT transducers

EMAT transducers are electromagnetic acoustic transducers that use Lorentz forces and/or magnetic as well as magnetostrictive forces to excite a wave within the part to be inspected. Using this principle, EMAT transducers do not require coupling or contact and also work through a thin layer of paint. Usually, EMATs consist of specifically designed induction coils which are based on, e.g., meandertype windings. Via induction, a current pulse sent through the coils generates eddy currents in the near-surface region of the component. Superposition of these eddy currents with a static magnetic field

which is perpendicular to the surface leads to periodically alternating Lorentz forces, generating a respective particle displacement at ultrasonic frequencies. The essential advantage of EMAT transducers is the non-contact generation of ultrasonic waves, with the possibility to directly excite shear waves with horizontal or vertical polarisation.

Fraunhofer IZFP started designing EMATs in the 1980s addressing one of the oldest and most frequent applications of EMATs, the measurement of wall thickness in the classical pulse echo technique [129]. In the field of nuclear inspection, the high degree of elastic anisotropy, the coarse grain structure of weld metal and buttering in austenitic and bimetallic welds raised the interest of using EMATs, since SH-waves are less affected by the mentioned complications than SV- and L-waves. Their better capability to penetrate into and to pass through the anisotropic weld has been experimentally demonstrated on some cases; in a wide range of angles of incidence (from 50° to 90°), nearly total transmission of the sound pressure from the austenitic base metal into the weld metal [130] was observed.

Due to the respective excitation mechanisms, currently available EMATs are restricted to relatively low frequencies of about 2.5 MHz for ferromagnetic materials and about 1 MHz for austenitic steels, resulting in a relatively low resolution in defect detection. EMAT transducers can also be designed as phased arrays [131], with respective steering and focusing capabilities. Over the years, EMAT technology and inspection equipment have been enhanced, addressing further applications, such as pipeline inspection [132]. Yet, further challenges such as operation at higher frequencies and/or at elevated temperatures still leave potential for further improvements [133].

6.1.3 Frequency and excitation signal

The choice of frequency as a trade-off between resolution and penetration depth is an elementary knowledge for the ultrasonic NDE practitioner. While experiments using excitation with continuous waves [134] have demonstrated that an optimal frequency range yielding the best signal to noise ratio for a given test depth can be determined, broadband transducers with a limited range of central frequencies (usually 1.5MHz and 2.25MHz) are used for the inspection of coarse grained materials in practice.

Few investigations have been made into the impact of the spectral composition of an ultrasonic pulse on the signal to noise ratio. However, it is admitted that a shorter pulse length not only increases axial resolution, but also reduces backscatter, owing to the reduction of the insonified volume. Highly damped transducers are therefore recommended for the inspection of coarse-grained materials.

Low or very low signal-to-noise ratio is not uncommon in ultrasonic inspection. One way to address this challenge is to use techniques belonging to the pulse compression family [135], [136]. In essence, they consist in transmitting a modulated pulse or a sequence of pulses and cross-correlating them with the reflected signals, so that their duration is compressed, and amplitude increased. Consequently, the energy of the received signal is maximised and good resolution maintained without the need for very high-power inputs. Coded sequences, which code the polarity of concatenated bursts according to a binary sequence, are particularly attractive for inspection scenarios [137]. However, a combination of low SNR and close proximity of reflectors posed a significant challenge in many applications. In recent years, a new approach, based on incorporating gaps in the coded sequence to allow for reception, has been proposed [138]. It was shown that using an equal number of transmitting and receiving intervals of the same length distributed randomly performs optimally. This technique enabled increasing SNR by more than 30 dB, outperforming averaging on both measurement duration and SNR improvement.

What is more, continuous transmission is also possible, leading to the reduction of the time needed for the system to respond to changes.

6.2 Configuration

6.2.1 Single crystal vs. phased array transducers

Conventional transducers use a single active piezo element, for which it is assumed that the entire surface is excited uniformly – this is sometimes referred to as piston mode. Phased array transducers consist of a number of small piezo elements, typically arranged in a line or a matrix, which can be pulsed independently. This allows to introduce individual delays to each transducer element, thereby controlling the resulting pattern of constructive interference. This allows beam steering and focusing and is also used by more advanced inspection techniques. All the configurations mentioned in the following subparagraphs can take advantage of phased array technology.

6.2.2 Single transducer configurations

The most simply and widely used configuration, commonly referred to as pulse-echo, uses the same transducer for transmission and reception of the signal. Since reception cannot begin until the transmission is entirely terminated, a pulse echo transducer has a blind time after the excitation before reception starts, although an appropriate choice of sound path in the coupling medium can limit the practical consequences. More importantly, single transducers are exposed to the backscatter generated by the sound beam, reducing signal to noise ratio and thus penetration depth.

6.2.3 Dual transducer configurations: TOFD

The TOFD technique originated in 1985 at the Harwell Center in the UK as a method to detect and size cracks in nuclear reactor welds [139]. TOFD stands for time of flight diffraction and refers to a configuration with separate and symmetrical transducers for transmission and reception, typically located on opposite sides of a weld. TOFD uses incidence angles between 45° and 70°, allowing to generate both a lateral wave and an oblique incidence wave. In the absence of a defect, the receiving transducer registers the lateral wave and the backwall reflection, while in the presence of a defect, diffraction echoes from one or both crack tips are also registered. The absence of the lateral wave signal or the backwall signal indicates the presence of a surface breaking defect.

The TOFD method has two inherent drawbacks: Due to the presence of a lateral wave, a dead zone of a few mm below the inspection surface is observed. Furthermore, since the method relies on diffraction signals, which are about 20 dB less than specularly reflected echoes, the method has limitated penetration depth in coarse grain materials.

6.2.4 Dual transducer configurations: TRL

A quite intuitive measure to reduce scatter during the acquisition phase is to use highly directional transducers that limit the volume of metal insonified. For welds and castings, the state-of-the-art technique is TRL (Transmission Reception Longitudinal), also known as SEL (Sende-Empfang Longitudinal), using separate transmitter and receiver elements on a wedge in a way that both beams overlap in a small zone at a given depth. While early designs with single transmitter and receiver elements required a number of different probes to cover a larger depth range (popular refraction angles being 55° and 70°), more recent phased array TRL probes (also called dual matrix array probes)

cover a larger depth range with a single probe (except for near surface defects) and provide the additional benefit of the ability to examine at a given depth with varying incidence angles.

Another advantage of the TRL design is that owing to the separation of transmitter and receiver, no damping material is necessary, resulting in a reduced wedge size and therefore overall higher sensitivity. The current state of the art is TRL matrix probes with 28 or 32 elements for each probe.

The longitudinal wave emitted by TRL transducers is accompanied by a transverse wave, which is converted to a longitudinal wave through reflection at the back wall, producing a secondary echo for a perpendicularly oriented defect at the backwall, which is more pronounced for lower incidence angles.

6.3 Acquisition

In the early days of NDT, the ultrasound signal was obtained as a time-record ("A-scan") on an analogue cathode ray screen. This was interpreted by the inspector and recorded manually. This concept remains and is heavily used in modern routine inspections, although the instrument, known as "Flaw Detector" is now digital and the information is recorded and stored in a digital format. Flaw detectors typically have options of either pulse-echo, using a single transducer, or pitch-catch, using one transducer to transmit and another to receive.

The advent of ultrasound array transducers for NDT brought the possibility of a totally new approach to NDT, enabling flexible uses to achieve focus and aperture control at different locations within the component, while using a single device. Initial uses of array transducers used pre-set "delay laws", whereby the inspector chose settings of the instrument to decide on the focal location in the component. This transformed the array transducer into a flexible transducer with variable focus but retained the familiar concept of inspection long-established with flaw detectors. However, the real potential of array transducers is realised only when the signals are acquired and stored from the individual array elements, for processing afterwards. This allows for processing after acquisition to focus at any, or all, locations in the component, to apply any choice of imaging algorithm, and to save a permanent record of all the signals that could be used for future review and further processing.

The acquisition of all signals of an array transducer so as to be able to achieve this potential has become known as “Full matrix capture” (FMC). For an array of N elements, each element is successively used as transmitter, while all other elements are used as receivers [140]. The acquired data is organised in a three-dimensional matrix containing every possible combination of transmitting and receiving elements. By convention, element Sij contains the signal transmitted by element i and received by element j.

6.4 Standards and specifications (Industry related)

This section discusses current or in progress standards and specifications that describe the practice of the examination / inspection of these difficult austenitic materials. General standards for ultrasonic examination are EN583 and ISO standard 17640, while ISO standard 10863 is dedicated to the specifics of time of flight diffraction.

The application of Phased Array technology for UT inspection of welded components is described by ISO standard 13588 [141], but this standard is limited to the consideration of low carbon alloy steel materials.

The inspection of welds in austenitic steels is governed in the EU by ISO standard 22825 [142], covering techniques, test blocks, procedure requirements etc. The standard explicitly distinguishes four cases:

- Fine grained weld, heat affected zone and parent metal, for which shear wave techniques can be used
- Fine grained parent metal and coarse-grained weld metal, where shear waves can only be applied for defects in the parent material or the fusion line, and compression waves for direct defect detection or mode converted waves for indirect insonification of reflectors must be used
- Coarse microstructure both in the parent metal and the weld, requiring compression waves using direct insonification
- Structures not allowing for UT inspection, due to insufficient signal to noise ratio

Annex A of ISO 22825 [142] lists as possible compression wave techniques for the inspection of austenitic welds

- Direct insonification with refracted compression waves, generating also shear waves through mode conversion before the first critical angle
- Indirect insonification with refracted compression waves via mode conversion
- Tandem technique with mode conversion (for vertical cracks)
- Creeping waves for near surface defects

The standard highlights the need for multiple angle probes to obtain full depth coverage, and explicitly mentions SEL-probes.

A working group, managed by International Institute of Welding (IIW) is in progress, to recommend application of UT with FMC / TFM. They intend to promote the adoption of good practice either at the manufacturing stage, for in-service inspection of existing plant or for repairs. The main applications considered deal with weld testing, welded defect characterization and sizing, damage assessment, forged or casting parts testing.

7 Imaging and inversion

This chapter of the report is devoted to the topics of imaging and inversion, as relevant to the scope of the ADVISE project. We will briefly review the current state of the art in imaging methods as well as inversion approaches. The development of these methods has gained considerable momentum with the advent of phased array transducers, which have rendered almost obsolete older techniques such as synthetic aperture focusing. Some of these techniques have their origins in radar applications, and many have first been applied in medical imaging.

7.1 Synthetic aperture focusing (SAFT)

Synthetic aperture focusing is arguably the oldest advanced imaging technique and exploits multiple transducer positions to increase the lateral resolution that would otherwise be obtained in a standard B-Scan image. In immersion setups with focused transducers, the lateral resolution is determined by the transducer aperture. SAFT combines scans from several adjacent positions, obtained during the displacement of the transducer, in order to create a virtual larger aperture with higher lateral resolution.

7.2 Total Focusing Method

Currently, the most common advanced imaging approach used in NDT is the Total Focusing Method (TFM) [143]. This method requires an ultrasonic transducer array, which is most often 1D (although other types of arrays are also in common use). The ultrasonic data at the core of the TFM imaging algorithm is a matrix of time domain signals that is obtained by emitting an ultrasonic pulse with every possible transmitter in a sequence and recording the signal received by all receivers for this emitting pulse. This acquisition scheme is known as the Full Matrix Capture (FMC). A high-quality image is then computed with a ray-based forward model by numerically focusing the time domain signals at every point of the region of interest. The obtained image is often superior to the classical B-scan or S-Scan images due to being optimally focused at every imaging point. Another advantage of TFM is that the focusing algorithm is applied to a set of signals that represents the impulse response matrix of the medium. This makes it possible to form any type of images by post-processing the same set of data, or to reduce noise or separate different kind of waves with advanced spatiotemporal filtering methods, such as the decomposition of the time reversal operator (DORT) method.

Since this imaging algorithm was introduced, it has been adapted successfully to several materials and contexts. Of particular interest to the ADVISE project is the body of work that seeks to apply TFM imaging to coarse grained materials [144] and highly attenuating materials [145]. These papers have shown that adequate filtering schemes based on the DORT method can significantly enhance TFM images by suppressing signals that introduce unwanted imaging artefacts, as well as separating defect contributions to the time domain data from noise. Another possible improvement demonstrated in [145] is the combination of coded emission techniques that diminish the electronic noise level and thus enhance the quality of the images.

Another general improvement to TFM imaging lies in the development of adaptive methods for irregular geometries [146]. These methods allow imaging below the surface of complex parts by a first imaging step dedicated to account for the scattering through the first interface below the probe. This

adaptive procedure is useful in industrial contexts and has since been implemented in industrial portable systems [147].

Another important aspect of TFM imaging is the ability to process the obtained image to propose defect characterization procedures. This can either take the form of processing that takes into account several different imaging modes (i.e. imaging paths that lead to different times of flight and hence map different signal locations to different parts of the image) to propose defect sizing [148] or of derived estimators such as the SEE estimator [149] which can be used to combine information from several individual images or be used to compensate a TFM image for more accurate sizing. The multi-mode imaging problem, i.e. how to optimally combine ultrasonic images that were reconstructed according to different paths, remains open, although several papers have advanced that topic in recent years [150]. In particular, existing work has highlighted the existence of non-physical indications related to ambiguous flight paths that may lead to misinterpretations [151].

In the scope of the ADVISE project, all of the techniques mentioned above will likely need to be combined: processing in the frequency domain, taking into account the properties of the materials, imaging below complex interfaces. Potential applications include but are not limited to: profile measurement of external as well as internal weld boundaries, in particular anisotropic welds; detection of defects located within the welded regions, for example when surface irregularities are present; detection of defects in noisy materials.

7.3 Plane Wave Imaging

Plane Wave Imaging (PWI) is an imaging procedure that has been introduced in recent years in the context of NDT [152], although it has been applied to medical imaging for quite some time. It can be seen as an improvement with respect to TFM because incident plane waves are limited diffraction beams that are not affected by spatial-spreading losses in the near-field of the array. Imaging with plane waves thus increases the signal-to-noise ratio in many cases. Since the number of emitted plane waves is usually smaller than the number of probe elements, the size of the acquired time domain data is also smaller compared to FMC data and thus takes less time to process in order to form an image, allowing frame rates of up to thousands of images per second in recent medical scanners.

Several enhancements of the PWI imaging are currently under active research. One of them is phase coherent imaging [153], a technique that can in certain case improve the signal to noise ratio.

Regarding the applications of PWI to NDT problems, the PhD thesis [154] presents images obtained with the DORT filter and the PWI imaging method on complex materials.

A last imaging method related to PWI imaging is the frequency domain imaging method [155]. Originally developed as an alternative to TFM image forming due to the computational efficiency of the Fourier transform, it has shown promise for fast imaging in 3D settings [156], and could be potentially hopeful for the estimation of the scattering matrix in the case of 3D defects.

In the scope of the ADVISE project, all of the techniques mentioned above related to PWI imaging will likely need to be combined: by also accounting for material properties, potential applications would again include profile measurement of external as well as internal weld boundaries, in particular anisotropic welds, detection of defects located within the welded regions, for example when surface irregularities are present, detection of defects in noisy materials.

7.4 Scattering coefficient matrix

In ultrasonic NDT, defect characterization approaches which make use of the scattering coefficient matrix (S-matrix) have been proposed as alternatives to image-based characterization. The defect S-matrix consists of far-field scattering coefficients of a defect for different incident/scattering angles, whose range is often determined by the defect location and array aperture size. It can be extracted from the experimental FMC data by using the sub-array imaging [157] or inverse imaging [158] approaches. The sub-array imaging approach works by applying TFM imaging to sub-array apertures of an array which helps to suppress the effect of measurement noise. The inverse imaging approach performs a forward imaging process that is reversible, and the scattering information of each defect can be extracted by applying spatial filtering to the image data, which gives both the amplitude and phase of the defect S-matrix.

The main advantage of these characterization methods lies in the fact that relatively small defects are better distinguishable from their scattering matrices than from an image. For example, it is shown in [159] that the half width at half maximum (HWHM, a feature describing the shape of an S-matrix) is sensitive to the crack size within the range [0.25λ, 2λ], and hence, has the potential to be used as an indicator of the crack size. However, this HWHM-based sizing approach has the limitation that it is only reliable when the specular reflection of a crack-like defect is measurable.

In more general approaches, S-matrix databases are formed and all the information of an S-matrix (instead of specific features such as the HWHM) is used for characterization. As a result, key parameters which are related to the defect geometry such as size, angle, and aspect ratio can be obtained by appropriate database searching approaches (e.g. based on a combination of similarity metrics [160]) or by classification [161]. These methods are shown to achieve good accuracy in experiments for idealized defect geometries including machined notches and volumetric elliptical voids. In addition, the effect of noise (including random noise and coherent noise due to defect roughness) is evaluated, and it is concluded that the performance of these characterization approaches is robust to noise given that the noise level is relatively low.

The defect manifold is a representation of the S-matrix database in principal-component space, and it contains the entirety of the available characterization information [162]. Besides providing a more intuitive way of understanding the defect characterization problem, the introduction of the defect manifold enables us to explore the statistical nature of the problem, i.e. the characterization uncertainty. More specifically, it can be shown using Bayes theorem that the probability distribution of defect parameters is related to measurement noise distribution. This also suggests that defect characterization can potentially become very challenging when the underlying noise level is high (e.g. due to multiple scattering effects from large grains). Using the uncertainty quantification technique developed in [162], it is shown through experiments that the defect aspect ratio can be determined accurately for a range of defects (including crack-like defects and volumetric voids), while the sizing results tend to have higher uncertainty. This issue can potentially be resolved by also using the phase and multiple-frequency information of the S-matrix as is demonstrated in [163].

In the scope of the ADVISE project, the techniques mentioned above can be used to characterize real defects which are found in complex structured materials. In particular, the effect of grain scattering can be studied by modelling S-matrices due to the grain noise. These techniques can also be used to optimize characterization, i.e. to design an array that does the best possible characterization for a certain measurement scenario.

7.5 Weld stiffness map inversion

The challenge of inspecting complex austenitic steel welds may be further complicated by some of the weld parameters being unknown. It is therefore attractive to use ultrasonic measurements for characterising the microstructure of the weld, which could then deliver a reliable baseline model for imaging. This arduous task relies on a model that predicts grain orientations either from geometry or from welding parameters. Despite large computational resources available nowadays, such a model should preferably rely on a small number of parameters, to maintain viability and not to rely on high performance clusters.

Several approaches to inversion have been recently reported in the literature. Gueudre *et al.* [5] used the MINA model to represent grain orientations and updated its parameters based on the echo-dynamic curve received along the base face of the weld. The parameters were fit using a genetic algorithm, achieving good agreement with experimental data. However, since this technique was based on measuring amplitude, it suffered from a number of issues such as attenuation, unaccounted for grain scattering and uncertain coupling of sensors. All these factors pose a significant challenge in practice. Another approach was suggested by Zhang *et al.* [150], who divided the weld according to a square grid and updated the orientation within each element, based on the measured time-of-flight. Whilst using time-of-flight circumvents the issues quoted above, the Markov-chain Monte Carlo approach to model updating incurs significant CPU requirements for a problem relying on a large number of parameters.

Combining the time-of-flight measurement with a small parameter space model was proposed by Fan *et al.* [97]. They based the inversion upon the MINA model, focusing on determining four parameters using time-of-flight measurements. Both transmitting and receiving arrays were placed on the top surface of the weld, so that the ultrasonic beam travelled through the weld, reflected from the backwall and propagated up to the top surface before being recorded. It was desirable to use only the shear wave, the most sensitive to orientation variations, which needed to be extracted from the received time histories using appropriate signal processing techniques. MINA parameters were updated using a genetic algorithm, achieving errors smaller than 20 degrees after 100 iterations (as compared to the macrograph). The results were promising, but several challenges remain open, such as more complex weld configurations, the effect of the third dimension, and the effect of grain size and distribution on measured signals.

7.6 Signal processing

One of the earliest signal processing techniques applied to increase the signal to noise ratio in bulk coarse grain materials is grain echo decorrelation [164], which uses averaging of pulse-echo signals obtained at slightly shifted transducer positions above a reflector.

More recently, filters on TFM imaging have been applied successfully by using the Decomposition of the Time Reversal Operator (DORT) method [165]. This method, initially used to eliminate the artefacts caused by the recorded surface waves, is also able to discriminate the contribution of the defect with a significant improvement of the SNR compared to the original TFM image.

8 Open challenges and conclusions

This document summarised important developments and achievements in the area of modelling and inspection of complex structured materials in recent decades. The advances have been significant and a plethora of models for both fundamental phenomena and more complex weld formation/inspection are available. However, to date the links between model predictions and in-situ characterisations were not established enough to allow for full model-assisted inspection.

While creating new inspection protocols by merging the expertise already possessed by the members of the ADVISE consortium is a promising initiative, there are several open challenges, deemed as critically important for enabling a step change in the development of the area. These challenges are grouped with respect to the topic headings below:

1 Weld modelling:
   - micro-scale weld modelling, capable of predicting grain size and distribution incurs prohibitive computational costs from the perspective of online characterisation;
   - small parameter weld models are only available for simple weld configurations and confined to 2D; there is a need for simplified models for a larger range of typical welds in the nuclear industry.

2 Wave propagation modelling:
   - fast computer models including the capability to fully take the micro-structure of a material into account need to be established; however, the most appropriate propagation and scatter models for this task are not clearly identified, nor is the required refinement of the structure's representation in the model;
   - the use of numerical models for characterisation and inspection needs to be further assessed, in the light of recent developments in the area of numerical computing, particularly parallelisation and graphical card-based solutions.

3 Characterisation:
   - little prior work on microstructure reconstruction from in-situ UT measurements exists;
   - only simple structures have been addressed in the existing literature on characterisation; weld map inversion for other configurations and three-dimensions, if needed, are open for investigation;
   - grain size and distribution reconstruction received very scarce attention to date; such predictions are necessary both for welds and cast components.

4 Experimental issues:
   - the performance benefits of EMAT transducer with respect to their capability to generate SH waves are not demonstrated;
   - the shape/spectrum of the most appropriate excitation signal is an open issue;
   - the choice of array transducer parameters, such as frequency and aperture, so as to optimise the inspection for signal to noise ratio, is still very poorly understood; the choice and parameters of imaging algorithms for best performance on detecting and characterising defects in strongly-scattering materials is a subject of ongoing research and is also not yet resolved.

The base of knowledge gathered in this report serves as a starting point for activities aimed at tackling the above-mentioned challenges in the course of the ADVISE project.

9 Bibliography

[1] K. E. Easterling, *Introduction to the physical metallurgy of welding*. Butterworth Heinemann, 1992.

[2] B. Chassignole, D. Villard, M. Dubuget, J.-C. Baboux, and R. E. Guerjouma, "Characterization of austenitic stainless steel welds for ultrasonic NDT," *AIP Conf. Proc.*, vol. 509, no. 1, pp. 1325–1332, May 2000.

[3] J. Moysan, A. Apfel, G. Corneloup, and B. Chassignole, "Modelling the grain orientation of austenitic stainless steel multipass welds to improve ultrasonic assessment of structural integrity," *Int. J. Press. Vessels Pip.*, vol. 80, no. 2, pp. 77–85, Feb. 2003.

[4] A. Apfel, J. Moysan, G. Corneloup, and B. Chassignole, "Simulations of the influence of the grains orientations on ultrasounds," in *16th WCNDT*, 2004.

[5] C. Gueudre, L. Le Marrec, J. Moysan, and B. Chassignole, "Direct model optimisation for data inversion. Application to ultrasonic characterisation of heterogeneous welds," *NDT E Int.*, vol. 42, no. 1, pp. 47–55, Jan. 2009.

[6] A. F. Mark, Z. Fan, F. Azough, M. J. S. Lowe, and P. J. Withers, "Investigation of the elastic/crystallographic anisotropy of welds for improved ultrasonic inspections," *Mater. Charact.*, vol. 98, pp. 47–53, Dec. 2014.

[7] W. Kurz, B. Giovanola, and R. Trivedi, "Theory of microstructural development during rapid solidification," *Acta Metall.*, vol. 34, no. 5, pp. 823–830, May 1986.

[8] R. J. Ditchburn, S. K. Burke, and C. M. Scala, "NDT of welds: state of the art," *NDT E Int.*, vol. 29, no. 2, pp. 111–117, Apr. 1996.

[9] B. Hosten, M. Deschamps, and B. R. Tittmann, "Inhomogeneous wave generation and propagation in lossy anisotropic solids. Application to the characterization of viscoelastic composite materials," *J. Acoust. Soc. Am.*, vol. 82, no. 5, pp. 1763–1770, Nov. 1987.

[10] J. A. Ogilvy, "Computerized ultrasonic ray tracing in austenitic steel," *NDT Int.*, vol. 18, no. 2, pp. 67–77, Apr. 1985.

[11] M. Spies, "Modeling of transducer fields in inhomogeneous anisotropic materials using Gaussian beam superposition," *NDT E Int.*, vol. 33, no. 3, pp. 155–162, Apr. 2000.

[12] K. J. Langenberg *et al.*, "Application of modeling techniques for ultrasonic austenitic weld inspection," *NDT E Int.*, vol. 33, no. 7, pp. 465–480, Oct. 2000.

[13] V. Schmitz, F. Walte, and S. V. Chakhlov, "3D ray tracing in austenite materials," *NDT E Int.*, vol. 32, no. 4, pp. 201–213, Jun. 1999.

[14] F. E. Stanke and G. S. Kino, "A unified theory for elastic wave propagation in polycrystalline materials," *J. Acoust. Soc. Am.*, vol. 75, no. 3, pp. 665–681, 1984.

[15] U. F. Kocks, C. N. Tomé, H.-R. Wenk, and A. J. Beaudoin, *Texture and Anisotropy: Preferred Orientations in Polycrystals and Their Effect on Materials Properties*. Cambridge University Press, 2000.

[16] R. Quey, P. R. Dawson, and F. Barbe, "Large-scale 3D random polycrystals for the finite element method: Generation, meshing and remeshing," *Comput. Methods Appl. Mech. Eng.*, vol. 200, no. 17, pp. 1729–1745, Apr. 2011.

[17] M. A. Groeber and M. A. Jackson, "DREAM.3D: A Digital Representation Environment for the Analysis of Microstructure in 3D," *Integrating Mater. Manuf. Innov.*, vol. 3, no. 1, p. 5, Apr. 2014.

[18] A. Van Pamel, C. R. Brett, P. Huthwaite, and M. J. Lowe, "Finite element modelling of elastic wave scattering within a polycrystalline material in two and three dimensions," *J. Acoust. Soc. Am.*, vol. 138, no. 4, pp. 2326–2336, 2015.

[19] M.-A. Ploix, P. Guy, R. Elguerjouma, J. Moysan, G. Corneloup, and B. Chassignole, “Attenuation assessment for NDT of austenitic stainless steel welds,” in *9th European Conference on NDT (ECNDT), Berlin*, 2006.

[20] V. Dorval, F. Jenson, G. Corneloup, and J. Moysan, “Accounting for structural noise and attenuation in the modeling of the ultrasonic testing of polycrystalline materials,” in *AIP Conference Proceedings*, 2010, vol. 1211, pp. 1309–1316.

[21] B. Chassignole, O. Dupond, T. Fouquet, and F. Rupin, “Ultrasonic backscattering in polycrystalline materials of PWR components,” in *AIP Conference Proceedings*, 2011, vol. 1335, pp. 1136–1143.

[22] M. Spies and H. Rieder, “Synthetic aperture focusing of ultrasonic inspection data to enhance the probability of detection of defects in strongly attenuating materials,” *NDT E Int.*, vol. 43, no. 5, pp. 425–431, 2010.

[23] M. Spies and H. Rieder, “Der Einfluss der Schallschwächung in Guss-und Verbundwerkstoffen auf die Schallfelder von Standard-und Gruppenstrahler-Prüfköpfen,” *DGZfP Hrsg Zerstörungsfreie Mater. DGZfP Berl.*, 2010.

[24] E. B. Christoffel, “Über die Fortpflanzung von Stößen durch elastische feste Körper,” *Ann. Mat. Pura Ed Appl. 1867-1897*, vol. 8, no. 1, pp. 193–243, Jan. 1877.

[25] S. I. Rokhlin, T. K. Bolland, and L. Adler, “Reflection and refraction of elastic waves on a plane interface between two generally anisotropic media,” *J. Acoust. Soc. Am.*, vol. 79, no. 4, pp. 906–918, Apr. 1986.

[26] J. A. Ogilvy, “A layered media model for ray propagation in anisotropic inhomogeneous materials,” *Appl. Math. Model.*, vol. 14, no. 5, pp. 237–247, May 1990.

[27] A. H. Harker, J. A. Ogilvy, and J. a. G. Temple, “Modeling ultrasonic inspection of austenitic welds,” *J. Nondestruct. Eval.*, vol. 9, no. 2–3, pp. 155–165, Sep. 1990.

[28] E. P. Papadakis, “15 - Ultrasonic Attenuation Caused by Scattering in Polycrystalline Media,” in *Physical Acoustics*, vol. 4, W. P. Mason, Ed. Academic Press, 1968, pp. 269–328.

[29] S. Hirsekorn, “The scattering of ultrasonic waves by polycrystals,” *J. Acoust. Soc. Am.*, vol. 72, no. 3, pp. 1021–1031, 1982.

[30] S. Hirsekorn, “The scattering of ultrasonic waves in polycrystalline materials with texture,” *J. Acoust. Soc. Am.*, vol. 77, no. 3, pp. 832–843, 1985.

[31] S. Hirsekorn, “Directional dependence of ultrasonic propagation in textured polycrystals,” *J. Acoust. Soc. Am.*, vol. 79, no. 5, pp. 1269–1279, 1986.

[32] S. Hirsekorn, “The scattering of ultrasonic waves by multiphase polycrystals,” *J. Acoust. Soc. Am.*, vol. 83, no. 4, pp. 1231–1242, 1988.

[33] R. L. Weaver, “Diffusivity of ultrasound in polycrystals,” *J. Mech. Phys. Solids*, vol. 38, no. 1, pp. 55–86, Jan. 1990.

[34] S. Hirsekorn, U. Rabe, D. Bruche, W. Arnold, N. Grov, and T. Kinzler, “High-frequency ultrasonic porosity testing of non-ferrous metal die castings,” *Cast. Plant Technol.*, vol. 4, p. 28, 2007.

[35] S. Hirsekorn, U. Rabe, D. Bruche, N. Grov, T. Kinzler, and W. Arnold, “Non-Destructive Testing of Die-Casting Components of Non-Ferrous Metals for Surface-Near Porosity by High-Frequency Ulrasound,” in *Acoustical Imaging*, Springer, Dordrecht, 2008, pp. 223–232.

[36] D. Dobrovolskij, S. Hirsekorn, and M. Spies, “Simulation of Ultrasonic Materials Evaluation Experiments Including Scattering Phenomena due to Polycrystalline Microstructure,” *Phys. Procedia*, vol. 70, pp. 644–647, 2015.

[37] L. Yang and S. I. Rokhlin, “Ultrasonic backscattering in cubic polycrystals with ellipsoidal grains and texture,” *J. Nondestruct. Eval.*, vol. 32, no. 2, pp. 142–155, 2013.

[38] S. I. Rokhlin, J. Li, and G. Sha, “Far-field scattering model for wave propagation in random media,” *J. Acoust. Soc. Am.*, vol. 137, no. 5, pp. 2655–2669, 2015.

[39] J. Li and S. I. Rokhlin, “Elastic wave scattering in random anisotropic solids,” *Int. J. Solids Struct.*, vol. 78–79, pp. 110–124, Jan. 2016.

[40] R. B. Thompson *et al.*, “Scattering of elastic waves in simple and complex polycrystals,” *Wave Motion*, vol. 45, no. 5, pp. 655–674, 2008.

[41] A. V. Pamel, G. Sha, S. I. Rokhlin, and M. J. S. Lowe, “Finite-element modelling of elastic wave propagation and scattering within heterogeneous media,” *Proc R Soc A*, vol. 473, no. 2197, p. 20160738, Jan. 2017.

[42] A. Van Pamel, G. Sha, M. J. S. Lowe, and S. I. Rokhlin, “Numerical and analytic modelling of elastodynamic scattering within polycrystalline materials,” *J. Acoust. Soc. Am.*, vol. 143, no. 4, pp. 2394–2408, Apr. 2018.

[43] M. G. Gustafsson and T. Stepinski, “Studies of split spectrum processing, optimal detection, and maximum likelihood amplitude estimation using a simple clutter model,” *Ultrasonics*, vol. 35, no. 1, pp. 31–52, Feb. 1997.

[44] S. Chatillon, “Simplified Modeling of Backscattered Noise and Attenuation Phenomena for Quantitative Performance Demonstration of UT Methods,” 2003, vol. 657, pp. 93–100.

[45] I. Yalda, F. J. Margetan, and R. B. Thompson, “Predicting ultrasonic grain noise in polycrystals: A Monte Carlo model,” *J. Acoust. Soc. Am.*, vol. 99, no. 6, pp. 3445–3455, Jun. 1996.

[46] V. Dorval, F. Jenson, G. Corneloup, and J. Moysan, “Simulation of structural noise and attenuation occurring in ultrasonic NDT of polycrystalline materials,” in *Ultrasonic Wave Propagation in Non Homogeneous Media*, Springer, Berlin, Heidelberg, 2009, pp. 365–375.

[47] R. B. Thompson and F. J. Margetan, “Use of elastodynamic theories in the stochastic description of the effects of microstructure on ultrasonic flaw and noise signals,” *Wave Motion*, vol. 36, no. 4, pp. 347–365, Oct. 2002.

[48] G. Ghoshal, J. A. Turner, and R. L. Weaver, “Wigner distribution of a transducer beam pattern within a multiple scattering formalism for heterogeneous solids,” *J. Acoust. Soc. Am.*, vol. 122, no. 4, pp. 2009–2021, Oct. 2007.

[49] P. Hu and J. A. Turner, “Contribution of double scattering in diffuse ultrasonic backscatter measurements,” *J. Acoust. Soc. Am.*, vol. 137, no. 1, pp. 321–334, Jan. 2015.

[50] R. B. Thompson and T. A. Gray, “A model relating ultrasonic scattering measurements through liquid–solid interfaces to unbounded medium scattering amplitudes,” *J. Acoust. Soc. Am.*, vol. 74, no. 4, pp. 1279–1290, Oct. 1983.

[51] L. Schmerr and J.-S. Song, *Ultrasonic nondestructive evaluation systems*. Springer, 2007.

[52] M. Darmon and S. Chatillon, “Main Features of a Complete Ultrasonic Measurement Model: Formal Aspects of Modeling of Both Transducers Radiation and Ultrasonic Flaws Responses,” *Open J. Acoust.*, vol. 3, no. 03, p. 43, 2013.

[53] R. K. Chapman, “Ultrasonic scattering from smooth flat cracks: An elastodynamic Kirchhoff diffraction theory,” CEGB Report, North Western Region NDT Applications Centre, NWR/SSD/82/0059/R, 1982.

[54] J. D. Achenbach, A. K. Gautesen, and H. McMaken, *Ray methods for waves in elastic solids: with applications to scattering by cracks*, vol. 14. Pitman advanced publishing program, 1982.

[55] M. Darmon, N. Leymarie, S. Chatillon, and S. Mahaut, “Modelling of scattering of ultrasounds by flaws for NDT,” in *Ultrasonic wave propagation in non homogeneous media*, Springer, 2009, pp. 61–71.

[56] M. Spies, “Kirchhoff evaluation of scattered elastic wavefields in anisotropic media,” *J. Acoust. Soc. Am.*, vol. 107, no. 5, pp. 2755–2759, 2000.

[57] V. Dorval, S. Chatillon, B. Lu, M. Darmon, and S. Mahaut, “A general Kirchhoff approximation for echo simulation in ultrasonic NDT,” in *AIP Conference Proceedings*, 2012, vol. 1430, pp. 193–200.

[58] G. Baskaran, K. Balasubramaniam, C. V. Krishnamurthy, and C. L. Rao, “Ray based model for the ultrasonic time-of-flight diffraction simulation of thin walled structure inspection,” *J. Press. Vessel Technol.*, vol. 127, no. 3, pp. 262–268, 2005.

[59] S. K. Nath, “Effect of variation in signal amplitude and transit time on reliability analysis of ultrasonic time of flight diffraction characterization of vertical and inclined cracks,” *Ultrasonics*, vol. 54, no. 3, pp. 938–952, 2014.

[60] M. Darmon, S. Chatillon, S. Mahaut, L. J. Fradkin, and A. Gautesen, “Simulation of disoriented flaws in a TOFD technique configuration using GTD approach,” in *AIP Conference Proceedings*, 2008, vol. 975, pp. 155–162.

[61] V. Zernov, L. Fradkin, and M. Darmon, “A refinement of the Kirchhoff approximation to the scattered elastic fields,” *Ultrasonics*, vol. 52, no. 7, pp. 830–835, 2012.

[62] B. Lü, M. Darmon, L. Fradkin, and C. Potel, “Numerical comparison of acoustic wedge models, with application to ultrasonic telemetry,” *Ultrasonics*, vol. 65, pp. 5–9, 2016.

[63] B. Lü, “Modélisation de la propagation et de l’interaction d’une onde acoustique pour la télémétrie de structures complexes,” PhD Thesis, Université du Maine, 2011.

[64] M. Darmon, V. Dorval, A. K. Djakou, L. Fradkin, and S. Chatillon, “A system model for ultrasonic NDT based on the physical theory of diffraction (PTD),” *Ultrasonics*, vol. 64, pp. 115–127, 2016.

[65] A. Kamta Djakou, M. Darmon, L. Fradkin, and C. Potel, “The Uniform geometrical Theory of Diffraction for elastodynamics: Plane wave scattering from a half-plane,” *J. Acoust. Soc. Am.*, vol. 138, no. 5, pp. 3272–3281, 2015.

[66] M. Darmon, P. Calmon, and B. Bèle, “An integrated model to simulate the scattering of ultrasounds by inclusions in steels,” *Ultrasonics*, vol. 42, no. 1, pp. 237–241, 2004.

[67] C. F. Ying and R. Truell, “Scattering of a plane longitudinal wave by a spherical obstacle in an isotropically elastic solid,” *J. Appl. Phys.*, vol. 27, no. 9, pp. 1086–1097, 1956.

[68] N. G. Einspruch, E. J. Witterholt, and R. Truell, “Scattering of a plane transverse wave by a spherical obstacle in an elastic medium,” *J. Appl. Phys.*, vol. 31, no. 5, pp. 806–818, 1960.

[69] M. H. Burden and J. D. Hunt, “Cellular and dendritic growth. II,” *J. Cryst. Growth*, vol. 22, no. 2, pp. 109–116, Apr. 1974.

[70] G. Duggan, M. Tong, and D. J. Browne, “An integrated meso-scale numerical model of melting and solidification in laser welding,” *IOP Conf. Ser. Mater. Sci. Eng.*, vol. 27, no. 1, p. 012077, 2012.

[71] T. Koseki, H. Inoue, Y. Fukuda, and A. Nogami, “Numerical simulation of equiaxed grain formation in weld solidification,” *Sci. Technol. Adv. Mater.*, vol. 4, no. 2, p. 183, Jan. 2003.

[72] D. J. Browne and J. D. Hunt, “A Fixed Grid Front-Tracking Model of the Growth of a Columnar Front and an Equiaxed Grain During Solidification of an Alloy,” *Numer. Heat Transf. Part B Fundam.*, vol. 45, no. 5, pp. 395–419, May 2004.

[73] M. Toloui and M. Militzer, “Phase Field Modelling of Microstructure Evolution in the HAZ of X80 Linepipe Steel,” pp. 323–328, Sep. 2012.

[74] W. J. Poole, M. Militzer, and T. Garcin, “An Integrated Model to Predict Microstructure and Mechanical Properties in the Heat Affected Zone for X80 Linepipe,” presented at the 2012 9th International Pipeline Conference, 2012, pp. 301–306.

[75] T. Takaki, T. Fukuoka, and Y. Tomita, “Phase-field simulation during directional solidification of a binary alloy using adaptive finite element method,” *J. Cryst. Growth*, vol. 283, no. 1, pp. 263–278, Sep. 2005.

[76] W. U. Mirihanage and D. J. Browne, “Combined analytical/numerical modelling of nucleation and growth during equiaxed solidification under the influence of thermal convection,” *Comput. Mater. Sci.*, vol. 46, no. 4, pp. 777–784, Oct. 2009.

[77] V. Pavlyk and U. Dilthey, “Simulation of weld solidification microstructure and its coupling to the macroscopic heat and fluid flow modelling,” *Model. Simul. Mater. Sci. Eng.*, vol. 12, no. 1, p. S33, 2004.

[78] T. M. Rodgers, J. A. Mitchell, and V. Tikare, “A Monte Carlo model for 3D grain evolution during welding,” *Model. Simul. Mater. Sci. Eng.*, vol. 25, no. 6, p. 064006, 2017.

[79] T. M. Rodgers, J. D. Madison, and V. Tikare, “Simulation of metal additive manufacturing microstructures using kinetic Monte Carlo,” *Comput. Mater. Sci.*, vol. 135, pp. 78–89, Jul. 2017.

[80] E. R. Homer, V. Tikare, and E. A. Holm, “Hybrid Potts-phase field model for coupled microstructural–compositional evolution,” *Comput. Mater. Sci.*, vol. 69, pp. 414–423, Mar. 2013.

[81] X. Chen, X. Chen, H. Xu, and B. Madigan, “Monte Carlo simulation and experimental measurements of grain growth in the heat affected zone of 304 stainless steel during multipass welding,” *Int. J. Adv. Manuf. Technol.*, vol. 80, no. 5–8, pp. 1197–1211, Sep. 2015.

[82] S. Sista, Z. Yang, and T. Debroy, “Three-dimensional monte carlo simulation of grain growth in the heat-affected zone of a 2.25Cr-1Mo steel weld,” *Metall. Mater. Trans. B*, vol. 31, no. 3, pp. 529–536, Jun. 2000.

[83] M. A. Jabbareh and H. Assadi, “Modeling of Grain Structure and Heat-Affected Zone in Laser Surface Melting Process,” *Metall. Mater. Trans. B*, vol. 44, no. 4, pp. 1041–1048, Aug. 2013.

[84] S. Chen, G. Guillemot, and C.-A. Gandin, “3D Coupled Cellular Automaton (CA)–Finite Element (FE) Modeling for Solidification Grain Structures in Gas Tungsten Arc Welding (GTAW),” *ISIJ Int.*, vol. 54, no. 2, pp. 401–407, 2014.

[85] W. Tan and Y. C. Shin, “Multi-scale modeling of solidification and microstructure development in laser keyhole welding process for austenitic stainless steel,” *Comput. Mater. Sci.*, vol. 98, pp. 446–458, Feb. 2015.

[86] S. Szávai, Z. Bézi, J. Dudra, and I. Méhész, “Modelling of Phased Array Ultrasonic Inspection of a Steam Generator Dissimilar Metal Weld,” *Procedia Struct. Integr.*, vol. 2, pp. 1015–1022, Jan. 2016.

[87] H. Granjon, *Fundamentals of Welding Metallurgy*, English ed. Cambridge, England: Woodhead Publishing, 1991.

[88] P. R. Stepanishen, “Transient radiation from pistons in an infinite planar baffle,” *J. Acoust. Soc. Am.*, vol. 49, no. 5B, pp. 1629–1638, 1971.

[89] P. R. Stepanishen, “The Time-Dependent Force and Radiation Impedance on a Piston in a Rigid Infinite Planar Baffle,” *J. Acoust. Soc. Am.*, vol. 49, no. 3B, pp. 841–849, 1971.

[90] M. Spies, “Semi-analytical elastic wave-field modeling applied to arbitrarily oriented orthotropic media,” *J. Acoust. Soc. Am.*, vol. 110, no. 1, pp. 68–79, Jul. 2001.

[91] M. Spies, “High-speed mathematical modeling of ultrasound propagation in cladded and welded components using Gaussian beam superposition,” in *Proceedings of the 1st International Conference on NDE in Relation to Structural Integrity for Nuclear and Pressurized Components*, Cambridge, UK, 1999, pp. 948–955.

[92] M. Spies, “Modeling transient radiation of ultrasonic transducers in anisotropic materials including wave attenuation,” *AIP Conf. Proc.*, vol. 615, no. 1, pp. 807–814, May 2002.

[93] M. Spies, “Efficient optimization of single and multiple element transducers for the inspection of complex-shaped components,” *NDT E Int.*, vol. 37, no. 6, pp. 455–459, Sep. 2004.

[94] M. Spies, “Modeling the Beam Fields of Circular and Rectangular, Flat and Focused Transducers Using Gaussian Beam Superposition,” *AIP Conf. Proc.*, vol. 820, no. 1, pp. 946–953, Mar. 2006.

[95] M. Spies, “Ultrasonic field modeling for immersed components using Gaussian beam superposition,” *Ultrasonics*, vol. 46, no. 2, pp. 138–147, May 2007.

[96] G. D. Connolly, M. J. S. Lowe, J. A. G. Temple, and S. I. Rokhlin, “The application of Fermat’s principle for imaging anisotropic and inhomogeneous media with application to austenitic steel weld inspection,” *Proc. R. Soc. Math. Phys. Eng. Sci.*, vol. 465, no. 2111, pp. 3401–3423, Nov. 2009.

[97] Z. Fan, A. F. Mark, M. J. S. Lowe, and P. J. Withers, “Nonintrusive estimation of anisotropic stiffness maps of heterogeneous steel welds for the improvement of ultrasonic array inspection,” *IEEE Trans. Ultrason. Ferroelectr. Freq. Control*, vol. 62, no. 8, pp. 1530–1543, Aug. 2015.

[98] G. D. Connolly, M. J. S. Lowe, J. a. G. Temple, and S. I. Rokhlin, “Correction of ultrasonic array images to improve reflector sizing and location in inhomogeneous materials using a ray-tracing model,” *J. Acoust. Soc. Am.*, vol. 127, no. 5, pp. 2802–2812, May 2010.

[99] O. Nowers, D. J. Duxbury, J. Zhang, and B. W. Drinkwater, “Novel ray-tracing algorithms in NDE: Application of Dijkstra and A$*$ algorithms to the inspection of an anisotropic weld,” *NDT E Int.*, vol. 61, pp. 58–66, Jan. 2014.

[100] O. Nowers, D. J. Duxbury, and B. W. Drinkwater, “Ultrasonic array imaging through an anisotropic austenitic steel weld using an efficient ray-tracing algorithm,” *NDT E Int.*, vol. 79, pp. 98–108, Apr. 2016.

[101] V. Cerveny, *Seismic Ray Theory*. Cambridge University Press, 2005.

[102] C. Chapman, *Fundamentals of Seismic Wave Propagation*. Cambridge University Press, 2004.

[103] N. Gengembre and A. Lhémery, “Pencil method in elastodynamics: application to ultrasonic field computation,” *Ultrasonics*, vol. 38, no. 1, pp. 495–499, Mar. 2000.

[104] A. Lhémery, P. Calmon, I. Lecœur-Taïbi, R. Raillon, and L. Paradis, “Modeling tools for ultrasonic inspection of welds,” *NDT E Int.*, vol. 33, no. 7, pp. 499–513, Oct. 2000.

[105] A. Gardahaut, K. Jezzine, and D. Cassereau, “Paraxial ray-tracing approach for the simulation of ultrasonic inspection of welds,” *AIP Conf. Proc.*, vol. 1581, no. 1, pp. 529–536, Feb. 2014.

[106] V. Vavryčuk, “Real ray tracing in anisotropic viscoelastic media,” *Geophys. J. Int.*, vol. 175, no. 2, pp. 617–626, Nov. 2008.

[107] J. Virieux, “P-SV wave propagation in heterogeneous media: Velocity-stress finite-difference method,” *Geophysics*, vol. 51, no. 4, pp. 889–901, 1986.

[108] R. Ludwig and W. Lord, “A finite-element formulation for the study of ultrasonic NDT systems,” *IEEE Trans. Ultrason. Ferroelectr. Freq. Control*, vol. 35, no. 6, pp. 809–820, 1988.

[109] F. Fellinger and K. J. Langenberg, “Numerical techniques for elastic wave propagation and scattering,” in *Elastic Waves and Ultrasonic Nondestructive Evaluation*, 1990, pp. 81–86.

[110] C. Tsogka, “Modélisation mathématique et numérique de la propagation des ondes élastiques tridimensionnelles dans des milieux fissurés,” PhD Thesis, Paris IX Dauphine, 1999.

[111] E. Bécache, P. Joly, and C. Tsogka, “Fictitious domains, mixed finite elements and perfectly matched layers for 2-d elastic wave propagation,” *J. Comput. Acoust.*, vol. 09, no. 03, pp. 1175–1201, Sep. 2001.

[112] E. Becache, P. Joly, and C. Tsogka, “A New Family of Mixed Finite Elements for the Linear Elastodynamic Problem,” *SIAM J. Numer. Anal.*, vol. 39, no. 6, p. 24, 2002.

[113] R. Clayton and B. Engquist, “Absorbing boundary conditions for acoustic and elastic wave equations,” *Bull. Seismol. Soc. Am.*, vol. 67, no. 6, pp. 1529–1540, Dec. 1977.

[114] J.-P. Berenger, “A perfectly matched layer for the absorption of electromagnetic waves,” *J. Comput. Phys.*, vol. 114, no. 2, pp. 185–200, Oct. 1994.

[115] P. Rajagopal, M. Drozdz, E. A. Skelton, M. J. S. Lowe, and R. V. Craster, “On the use of absorbing layers to simulate the propagation of elastic waves in unbounded isotropic media using commercially available Finite Element packages,” *NDT E Int.*, vol. 51, pp. 30–40, Oct. 2012.

[116] P. Huthwaite, “Accelerated finite element elastodynamic simulations using the GPU,” *J. Comput. Phys.*, vol. 257, pp. 687–707, Jan. 2014.

[117] J. R. Pettit, A. Walker, P. Cawley, and M. J. S. Lowe, “A Stiffness Reduction Method for efficient absorption of waves at boundaries for use in commercial Finite Element codes,” *Ultrasonics*, vol. 54, no. 7, pp. 1868–1879, Sep. 2014.

[118] A. Van Pamel, P. B. Nagy, and M. J. S. Lowe, “On the dimensionality of elastic wave scattering within heterogeneous media,” *J. Acoust. Soc. Am.*, vol. 140, no. 6, pp. 4360–4366, Dec. 2016.

[119] A. T. Patera, “A spectral element method for fluid dynamics: Laminar flow in a channel expansion,” *J. Comput. Phys.*, vol. 54, no. 3, pp. 468–488, Jun. 1984.

[120] G. Seriani, E. Priolo, J. Carcione, and E. Padovani, “High-order spectral element method for elastic wave modeling,” in *SEG Technical Program Expanded Abstracts 1992*, 0 vols., Society of Exploration Geophysicists, 1992, pp. 1285–1288.

[121] G. Cohen, P. Joly, and N. Tordjman, “Construction and analysis of higher-order finite elements with mass lumping for the wave equation,” in *Proceedings of the second international conference on mathematical and numerical aspects of wave propagation*, 1993, pp. 152–160.

[122] G. Cohen, P. Joly, and N. Tordjman, “Higher-order finite elements with mass-lumping for the 1D wave equation,” *Finite Elem. Anal. Des.*, vol. 16, no. 3, pp. 329–336, Jun. 1994.

[123] D. Komatitsch, “Méthodes spectrales et éléments spectraux pour l’équation de l’élastodynamique 2D et 3D en milieu hétérogène,” PhD Thesis, Institut de physique du globe de paris-IPGP, 1997.

[124] G. Cohen, *Higher-Order Numerical Methods for Transient Wave Equations*. Berlin Heidelberg: Springer-Verlag, 2002.

[125] J. De Basabe and M. Sen, “Grid dispersion and stability criteria of some common finite-element methods for acoustic and elastic wave equations,” *GEOPHYSICS*, vol. 72, no. 6, pp. T81–T95, Oct. 2007.

[126] S. Imperiale, “Modélisation mathématique et numérique de capteurs piézoélectriques,” PhD Thesis, Université Paris-Dauphine, France, 2012.

[127] F. Casadei, E. Gabellini, G. Fotia, F. Maggio, and A. Quarteroni, “A mortar spectral/finite element method for complex 2D and 3D elastodynamic problems,” *Comput. Methods Appl. Mech. Eng.*, vol. 191, no. 45, pp. 5119–5148, Oct. 2002.

[128] C. Carrascal-Manzanare, A. Imperiale, G. Rougeron, V. Bergeaud, and L. Lacassagne, “A Fast Implementation of a Spectral Finite Elements Method on CPU and GPU Applied to Ultrasound Propagation,” in *Advances in Parallel Computing*, 2017, vol. 32, pp. 339–348.

[129] Wilbrand, A., “Quantitative modeling and experimental analysis of the physical properties of electromagnetic-ultrasonic transducers,” in *Review of Progress in Quantitative Nondestructive Evaluation*, 1988, vol. 7A, pp. 671–680.

[130] H. J. Salzburger and G. Huebschen, “UT of austenitic welds and cladding using electromagnetically excited SH-waves,” in *Review of Progress in Quantitative Nondestructive Evaluation*, 1986, vol. 5A, pp. 1687–1695.

[131] G. Hübschen and H. J. Salzburger, “Inspection of dissimilar metal welds using horizontally polarized shear (SH-) waves and electromagnetic ultrasonic (EMUS-) probes,” *Int. J. Press. Vessels Pip.*, vol. 39, no. 4, pp. 331–344, 1989.

[132] P. Jackel and F. Niese, “EMAT Application: Corrosion Detection with Guided Waves in Rod, Pipes and Plates,” in *Proceedings of the 11th European Conference on Non-Destructive Testing*, Prague, Czech, 2014, pp. 6–10.

[133] K. Sawaragi, H. J. Salzburger, G. Hübschen, K. Enami, A. Kirihigashi, and N. Tachibana, “Improvement of SH-wave EMAT phased array inspection by new eight segment probes,” *Nucl. Eng. Des.*, vol. 198, no. 1, pp. 153–163, May 2000.

[134] W. Oppermann and H.-A. Crostack, “Grundlegende Aspekte bei der Ultraschall-Prüfung von schallstreuenden Werkstoffen mit Signalen der CS-Technik,” *Mater. Werkst.*, vol. 12, no. 3, pp. 96–104, Mar. 1981.

[135] T. H. Gan, D. A. Hutchins, D. R. Billson, and D. W. Schindel, “The use of broadband acoustic transducers and pulse-compression techniques for air-coupled ultrasonic imaging,” *Ultrasonics*, vol. 39, no. 3, pp. 181–194, Apr. 2001.

[136] K. S. Ho, T. H. Gan, D. R. Billson, and D. A. Hutchins, “Application of pulse compression signal processing techniques to electromagnetic acoustic transducers for noncontact thickness measurements and imaging,” *Rev. Sci. Instrum.*, vol. 76, no. 5, p. 054902, Apr. 2005.

[137] M. Ricci, L. Senni, and P. Burrascano, “Exploiting Pseudorandom Sequences to Enhance Noise Immunity for Air-Coupled Ultrasonic Nondestructive Testing,” *IEEE Trans. Instrum. Meas.*, vol. 61, no. 11, pp. 2905–2915, Nov. 2012.

[138] J. Isla and F. Cegla, “Coded Excitation for Pulse-Echo Systems,” *IEEE Trans. Ultrason. Ferroelectr. Freq. Control*, vol. 64, no. 4, pp. 736–748, Apr. 2017.

[139] J. P. Charlesworth, *Engineering Applications of Ultrasonic Time-of-flight Diffraction*, 2nd Revised edition edition. Baldock, Hertfordshire, England; Philadelphia, Pa: Wiley-Blackwell, 2001.

[140] C. Holmes, B. W. Drinkwater, and P. D. Wilcox, “Post-processing of the full matrix of ultrasonic transmit–receive array data for non-destructive evaluation,” *NDT E Int.*, vol. 38, no. 8, pp. 701–711, Dec. 2005.

[141] ISO 13588:2012, “Non-destructive testing of welds — Ultrasonic testing — Use of automated phased array technlogy,” International Organization for Standardization, Oct. 2012.

[142] ISO 22825:2017, “Non-destructive testing of welds — Ultrasonic testing — Testing of welds in austenitic steels and nickel-based alloys,” International Organization for Standardization, Sep. 2017.

[143] C. Holmes, B. W. Drinkwater, and P. D. Wilcox, “Post-processing of the full matrix of ultrasonic transmit–receive array data for non-destructive evaluation,” *NDT E Int.*, vol. 38, no. 8, pp. 701–711, Dec. 2005.

[144] E. Lopez Villaverde, S. Robert, and C. Prada, “Ultrasonic imaging of defects in coarse-grained steels with the decomposition of the time reversal operator,” *J. Acoust. Soc. Am.*, vol. 140, no. 1, pp. 541–550, 2016.

[145] E. L. Villaverde, S. Robert, and C. Prada, “Ultrasonic Imaging in Highly Attenuating Materials With Hadamard Codes and the Decomposition of the Time Reversal Operator,” *IEEE Trans. Ultrason. Ferroelectr. Freq. Control*, vol. 64, no. 9, pp. 1336–1344, 2017.

[146] L. Le Jeune, S. Robert, P. Dumas, A. Membre, and C. Prada, “Adaptive ultrasonic imaging with the total focusing method for inspection of complex components immersed in water,” in *AIP Conference Proceedings*, 2015, vol. 1650, pp. 1037–1046.

[147] F. Reverdy, G. Benoist, and L. Le Ber, “Advantages and Complementarity of Phased-Array Technology and Total Focusing Method,” presented at the 19th World Conference on Non-Destructive Testing, 2016.

[148] K. Sy, “Étude et développement de méthodes de caractérisation de défauts basées sur les reconstructions ultrasonores TFM,” Paris Saclay, 2018.

[149] K. Sy, P. Bredif, E. Iakovleva, O. Roy, and D. Lesselier, “Development of the Specular Echoes Estimator to predict relevant modes for Total Focusing Method imaging,” 2017.

[150] J. Zhang, A. Hunter, B. W. Drinkwater, and P. D. Wilcox, “Monte carlo inversion of ultrasonic array data to map anisotropic weld properties,” *IEEE Trans. Ultrason. Ferroelectr. Freq. Control*, vol. 59, no. 11, pp. 2487–2497, Nov. 2012.

[151] E. Iakovleva, S. Chatillon, P. Bredif, and S. Mahaut, “Multi-mode TFM imaging with artifacts filtering using CIVA UT forwards models,” *AIP Conf. Proc.*, vol. 1581, no. 1, pp. 72–79, Feb. 2014.

[152] L. Le Jeune, S. Robert, E. Lopez Villaverde, and C. Prada, “Plane Wave Imaging for ultrasonic non-destructive testing: Generalization to multimodal imaging,” *Ultrasonics*, vol. 64, pp. 128–138, Jan. 2016.

[153] J. F. Cruza, J. Camacho, and C. Fritsch, “Plane-wave phase-coherence imaging for NDE,” *NDT E Int.*, vol. 87, pp. 31–37, Apr. 2017.

[154] E. Lopez Villaverde, “Imagerie ultrasonore dans des matériaux complexes par focalisation en tous points: développement d’une méthode de débruitage des images basées sur la décomposition de l’opérateur de retournement temporel,” Université Paris Diderot, 2017.

[155] A. J. Hunter, B. W. Drinkwater, and P. D. Wilcox, “The wavenumber algorithm for full-matrix imaging using an ultrasonic array,” *IEEE Trans. Ultrason. Ferroelectr. Freq. Control*, vol. 55, no. 11, pp. 2450–2462, Nov. 2008.

[156] L. Merabet, S. Robert, and C. Prada, “Development and evaluation of f-k migration methods for fast ultrasonic imaging in solids,” in *2016 IEEE International Ultrasonics Symposium (IUS)*, 2016, pp. 1–4.

[157] J. Zhang, B. W. Drinkwater, and P. D. Wilcox, “Defect characterization using an ultrasonic array to measure the scattering coefficient matrix,” *IEEE Trans. Ultrason. Ferroelectr. Freq. Control*, vol. 55, no. 10, pp. 2254–2265, Oct. 2008.

[158] A. Velichko and P. D. Wilcox, “Reversible back-propagation imaging algorithm for postprocessing of ultrasonic array data,” *IEEE Trans. Ultrason. Ferroelectr. Freq. Control*, vol. 56, no. 11, pp. 2492–2503, Nov. 2009.

[159] J. Zhang, B. W. Drinkwater, and P. D. Wilcox, “The Use of Ultrasonic Arrays to Characterize Crack-Like Defects,” *J. Nondestruct. Eval.*, vol. 29, no. 4, pp. 222–232, Dec. 2010.

[160] L. Bai, A. Velichko, and B. W. Drinkwater, “Ultrasonic characterization of crack-like defects using scattering matrix similarity metrics,” *IEEE Trans. Ultrason. Ferroelectr. Freq. Control*, vol. 62, no. 3, pp. 545–559, Mar. 2015.

[161] L. Bai, A. Velichko, and B. W. Drinkwater, “Characterization of defects using ultrasonic arrays: a dynamic classifier approach,” *IEEE Trans. Ultrason. Ferroelectr. Freq. Control*, vol. 62, no. 12, pp. 2146–2160, Dec. 2015.

[162] A. Velichko, L. Bai, and B. W. Drinkwater, “Ultrasonic defect characterization using parametric-manifold mapping,” *Proc R Soc A*, vol. 473, no. 2202, p. 20170056, Jun. 2017.

[163] L. Bai, A. Velichko, and B. W. Drinkwater, “Ultrasonic defect characterisation—Use of amplitude, phase, and frequency information,” *J. Acoust. Soc. Am.*, vol. 143, no. 1, pp. 349–360, Jan. 2018.

[164] S. Kraus and K. Goebbels, “Improvement of signal-to-noise ratio for the ultrasonic testing of coarse grained materials by signal averaging techniques,” in *Proceedings of the First International Symposium on Ultrasonic Material Characterization*, 1978, vol. 104.

[165] E. Lopez Villaverde, S. Robert, and C. Prada, “Ultrasonic imaging of defects in coarse-grained steels with the decomposition of the time reversal operator,” *J. Acoust. Soc. Am.*, vol. 140, no. 1, pp. 541–550, 2016.

10 Annex – Mock-up inventory

This annex contains a brief summary of the available mock-ups. A more detailed document is available on the project's SharePoint site for internal purposes only and will evolve throughout the project.

10.1 Weld mock-ups

The inventory of weld mock-ups is composed of 6 different families, with various degrees of complexity. Families 1 to 5 are planar mock-ups, supposedly representative of actual components, destined to be used during the development phase of the project, and essentially provided by EDF. Family 6 contains actual components, provided by Framatome and UJV, and destined for use in the validation phase of the project.

#	Family	Structure complexity	Description	Number of mock-ups	What changes between mock-ups?
1	**Weld mold**	★ ★ ↓ ★ ★ ★	Academic weld of large volume in order to obtain a highly homogeneous structure – Different welding conditions investigated	6	Welding conditions
2	**Model V-shape welds** « Primary pipe replacement weld »	★ ↓ ★ ★ ★	30 mm thick V-shape weld in various welding conditions and position – Large variety of defect	17	Welding position + Welding conditions
3	**Weld repair** « Tray-shape weld »	★ ↓ ★ ★ ★	15mm thick tray-shaped weld in flat and horizontal vertical welding position leading to a rather homogeneous structure – with buried notch underlying	9	Welding position + Welding process
4	**Medium thickness V-shape weld** « Surge line weld »	★ ★ ↓ ★ ★ ★	40mm thick V-shape welds done with manual shielded metal arc welding in various position – up to vertical rising position	14	Welding position
5	**Thick K-shape weld** « RCV nozzle weld »	★ ★ ↓ ★ ★ ★	70mm thick K-shape SMAW weld with various defects	4	Defects
6	**Pipe welds**	★ ★ ★	Actual welds in pipes with various geometries	16	Defects, Geometry

10.2 Coarse grained bulk material

The inventory of coarse-grained bulk material samples is composed of five families. Family 1 contains homogeneous samples of bulk material that was thermally treated to obtain different grain sizes. Families 2 and 3 contain centrifugally and static cast samples, and family 4 actual cast austenitic stainless-steel components. A fifth family contains forged stainless-steel blocks.

#	Family	Structure complexity	Description	Number of mock-ups	What changes between mock-ups?
1	**Coarse grained**	★	Thermally treated Ni-based alloys With different average grain sizes	9	Average grain size
2	**Centrifugally cast**	★★	Cylindrical blocks (portions of pipes) With notches and cracks	4	Structure and grain distribution
3	**Static cast**	★★	Rectangular blocks with mostly homogeneous Grain size, some columnar and equiaxed grains With and without defects (mostly SDH) Many with available macrographs	17	Structure and grain distribution
4	**CASS components**	★★★	Cast Stainless steel block	1	Structure, geometry, Grain distribution
5	**Forged stainless steel**	★★★	Portions of pipes, with side drilled holes and flat-bottomed holes	3	Geometry, reflectors